Graduate School ETD Form 9
(Revised 12/07)

PURDUE UNIVERSITY
GRADUATE SCHOOL
Thesis/Dissertation Acceptance

This is to certify that the thesis/dissertation prepared

By Woo-Suhl Cho

Entitled
Investigation of Homo-junction InGaAs Band-to-Band Tunneling Diodes

For the degree of Master of Science in Electrical and Computer Engineering

Is approved by the final examining committee:

GERHARD KLIMECK
Chair

MARK S. LUNDSTROM

RAMIRO EDWIN GARCIA

To the best of my knowledge and as understood by the student in the *Research Integrity and Copyright Disclaimer (Graduate School Form 20)*, this thesis/dissertation adheres to the provisions of Purdue University's "Policy on Integrity in Research" and the use of copyrighted material.

Approved by Major Professor(s): GERHARD KLIMECK

Approved by: M. R. Melloch 07-25-2011
Head of the Graduate Program Date

Graduate School Form 20
(Revised 6/09)

PURDUE UNIVERSITY
GRADUATE SCHOOL

Research Integrity and Copyright Disclaimer

Title of Thesis/Dissertation:

Investigation of Homo-junction InGaAs Band-to-Band Tunneling Diodes

For the degree of Master of Science in Electrical and Computer Engineering

I certify that in the preparation of this thesis, I have observed the provisions of *Purdue University Executive Memorandum No. C-22,* September 6, 1991, *Policy on Integrity in Research.**

Further, I certify that this work is free of plagiarism and all materials appearing in this thesis/dissertation have been properly quoted and attributed.

I certify that all copyrighted material incorporated into this thesis/dissertation is in compliance with the United States' copyright law and that I have received written permission from the copyright owners for my use of their work, which is beyond the scope of the law. I agree to indemnify and save harmless Purdue University from any and all claims that may be asserted or that may arise from any copyright violation.

Woo-Suhl Cho

Printed Name and Signature of Candidate

06-30-2011

Date (month/day/year)

*Located at http://www.purdue.edu/policies/pages/teach_res_outreach/c_22.html

INVESTIGATION OF HOMO-JUNCTION INGAAS BAND-TO-BAND TUNNELING DIODES

A Thesis

Submitted to the Faculty

of

Purdue University

by

Woo-Suhl Cho

In Partial Fulfillment of the

Requirements for the Degree

of

Master of Science in Electrical and Computer Engin

August 2011

Purdue University

West Lafayette, Indian

To my parents, Cho, Hee-Hyung and Lee, Hee-Ja

.

ACKNOWLEDGMENTS

I would like to thank my advisor, Professor Gerhard Klimeck, for providing me the opportunity to learn and work in his group with all the required resources for the research. I also thanks to Prof. Lundstrom and Prof. Garcia for being on my advisory committee. Special thank to Mathieu Luisier for his advice and guidance on my research. He also has been a good mentor and a friend to me. I would like to express my gratitude to all the colleagues in DLRC (specially to Hoon Ryu), my family, and all my friends for their help and support. I am also thankful to all the people who taught me what the life is: Y.M, B.K, S.H, J.A, M.H, Y.S, and J.R, J.Y, S.H, S.R, S.L, J.H, Y.T, J.S, H.S, I.J, I.G, S.M.

Thanks to Semiconductor Research Corporation and Intel for funding me and supporting my graduate studies.

TABLE OF CONTENTS

Page

LIST OF TABLES

LIST OF FIGURES

Figure Page

Figure Page

ABSTRACT

Cho, Woo-Suhl. M.S.E.C.E., Purdue University, August 2011. Investigation of homo-junction InGaAs band-to-band tunneling diodes. Major Professor: Gerhard Klimeck.

Band-to-band tunneling transistors (TFETs) are very promising devices to replace the conventional MOSFETs at the end of the semiconductor road map and to reduce the power consumption of integrated circuits due to their less than 60 mV/dec subthreshold swing. By investigating band-to-band tunneling (BTBT) diodes with a vertically grown p-n interface, it is possible to test the tunneling properties of a given material and its potential as TFETs.

Homo-junction InGaAs p-n tunneling diodes lattice matched to InP were investigated using a full-band and atomistic quantum transport approach based on the tight-binding model and the Non-equilibrium Green's Function (NEGF) formalism. Experimental devices fabricated at Penn State University and at Notre Dame University were considered.

A careful investigation of the available experimental data, especially the turn-on of the thermionic diode current suggested that band gap narrowing (BGN) plays an important role in heavily-doped BTBT diodes. Hence, this effect is included in the tight-binding model by altering its parameters according to the Jain-Roulston model, which calculates conduction and valence band shifts of n- and p- side of the diodes as function of doping concentration. BGN is then taken into account in the quantum transport simulations, and its effect on the current-voltage characteristics of the considered devices is analyzed. A good agreement with the available experimental data is obtained, both in the Zener and in the NDR side of the diodes. Future inclusions of electron-phonon scattering will help improve the remaining discrepancy between the experimental and simulation results in the valley current region.

1. INTRODUCTION

1.1. Moore's Law and Downscaling of MOSFETs

The Moore's law states that the number of transistors on an integrated circuit (IC) doubles about every two years. This has been continued due to the downscaling of Metal-oxide-semiconductor field-effect transistors (MOSFETs) and development of CMOS technology that lead to the performance improvement and cost reduction of transistors.

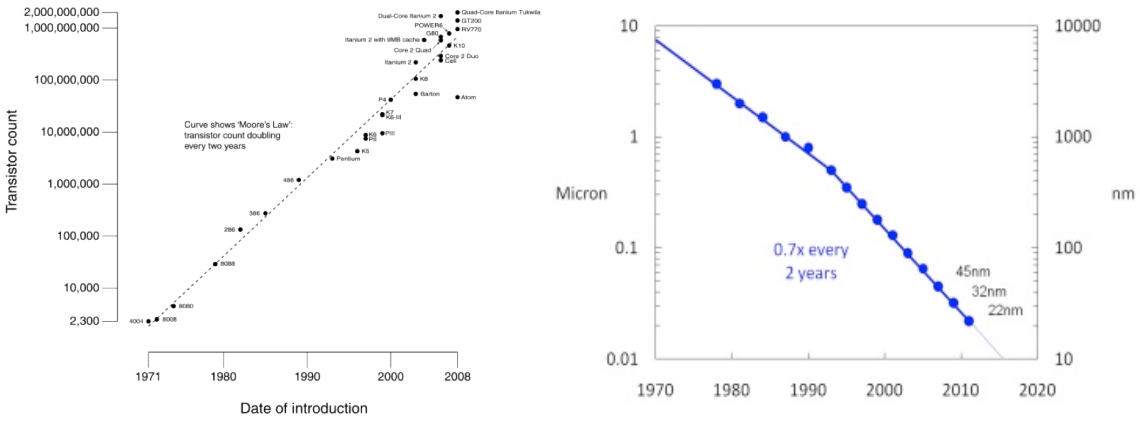

(a) (b)

Fig. 1.1 (a) The transistor counts from 1971 to 2008 followed by Moore's law [1] (b) The decrease of transistor dimensions corresponding to (a) [2]

Fig. 1.1 shows that the number of transistors has been increased followed by Moore's law, and the transistor dimensions have been decreased accordingly. However, the downscaling of MOSFETs has lead to a drastic increase of their power consumption and an unmanageable heat generation due to sub-threshold leakage currents and a non-scalable supply voltage.

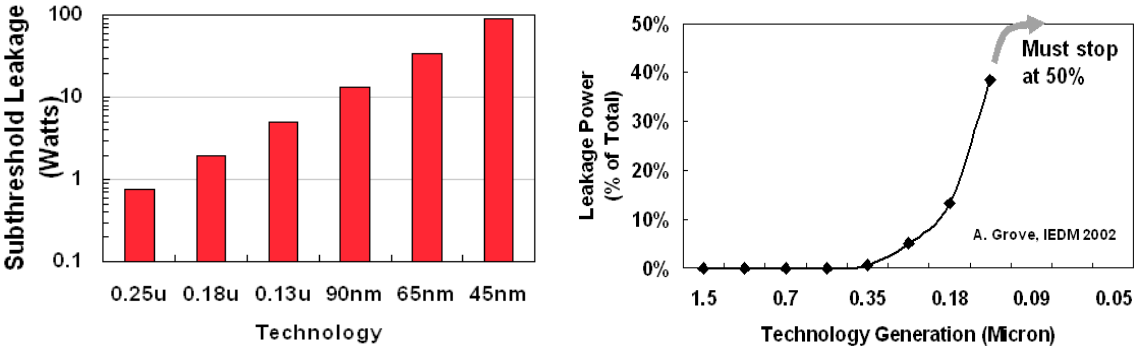

(a) (b)

Fig. 1.2 (a) The increase of sub-threshold leakage power as the size of CMOS decreases (b) The sub-threshold leakage power as a percentage of total power [3]

Fig. 1.2 shows that sub-threshold leakage power keeps increasing and taking the large portion of the total power as the CMOS dimensions are reduced. Since the number of transistors per chip increases followed by Moore's law, the leakage power also grows accordingly. Therefore, for the further continuation of Moore's law, the power consumption of transistors should be reduced while the transistor performance must keep increasing.

1.2. Limitations of MOSFET Scaling

The leakage power follows the equation,

$$P = I_{off} V_{DD} \tag{1.1}$$

where V_{DD} is a supply voltage, which must decrease to reduce the leakage power. To get high on-current and maintain high performance, the threshold voltage (V_T) also should decrease, which in turn exponentially increases the leakage current by following equations. Therefore, the downscaling of supply voltage is limited.

$$I_{ON} \propto (V_{DD} - V_T)^{\eta}, 1 \le \eta < 2 \tag{1.2}$$

$$I_{OFF} \propto e^{-\frac{V_T}{SS}} \tag{1.3}$$

However, in equation 1.3, there is another factor, which can affect the leakage current: SS called sub-threshold swing.

$$SS = \left(\frac{d \log I_d}{dV_g} \right)^{-1} = 2.3 \frac{kT}{q} \left(1 + \frac{C_d}{C_{ox}} \right) \geq 2.3 \frac{kT}{q} \simeq 60 mV/decade \tag{1.4}$$

The reduction of SS will decrease leakage current but this value is constrained by the physical limit of 60mV/decade. In MOSFETs, the current flows by diffusion of carriers over the source potential barrier controlled by gate, and the carrier concentration has an exponential function of energy. Fig. 1.3 illustrates this exponential sub-threshold characteristic.

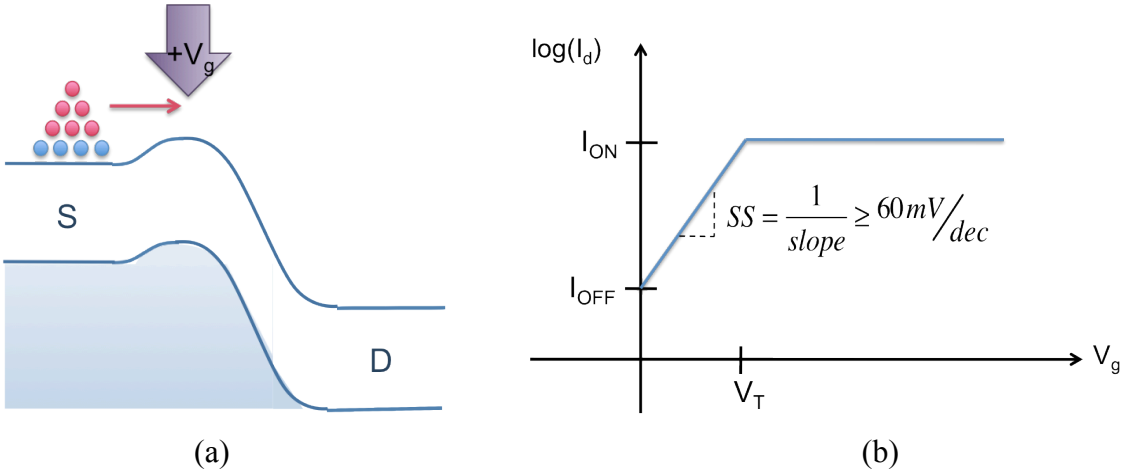

Fig. 1.3 (a) Exponential distribution of hot carriers (b) I_d vs. V_g curve for nMOSFET

1.3. Need for the New Device

Over the past twenty years, the development of CMOS technology has led to the downscaling of MOSFETs and therefore the increased packaging density. However, this improvement also has yielded the increase of power dissipation and heat generation in IC modules. Since energy efficiency is one of the biggest issues in the 21st century, transistors that can help reduce the power consumption of IC are highly desirable.

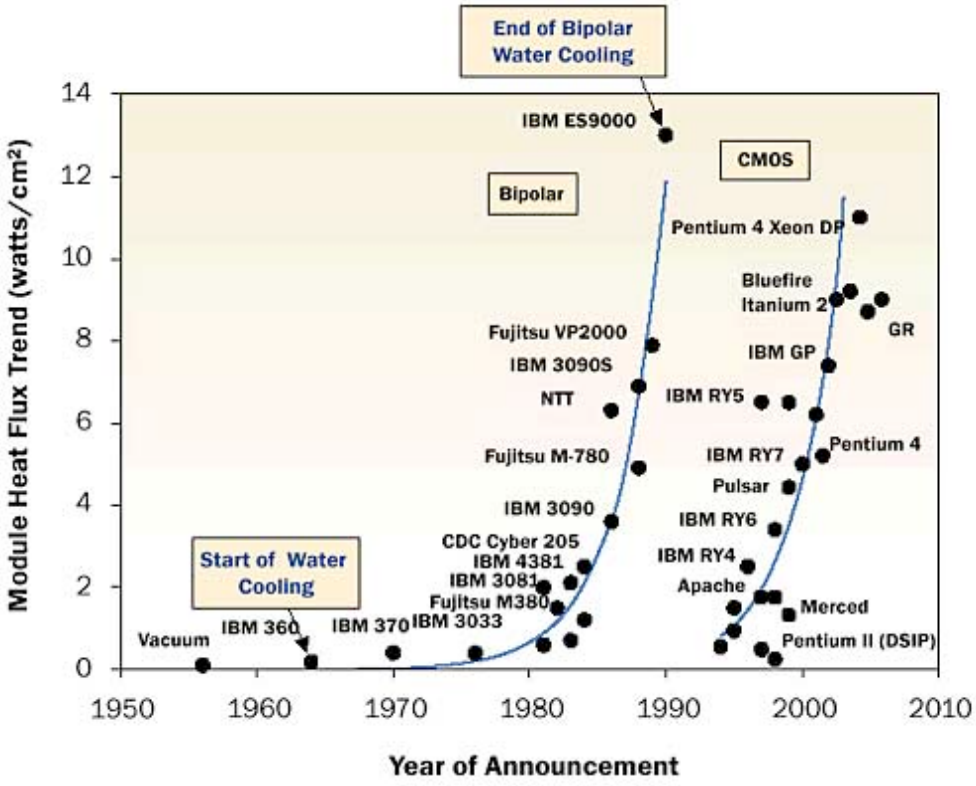

Fig. 1.4 Module heat flux trend for last fifty years [4]

Fig. 1.4 shows the module heat flux trend for last fifty years. During this time, BJTs (Bipolar Junction Transistors) are replaced by MOSFETs in order to limit the magnitude of the heat generation in a chip. However, CMOS technology no longer offers the power savings, and has reached the maximum power dissipation level that BJT had. Therefore, to continue the Moore's law, a shift of device technology is required.

Band-to-band tunneling (BTBT) field-effect transistors (TFETs), due to the injection of cold electrons through a potential barrier as described in the Fig. 1.5, can exhibit SS below the kT/q limit of MOSFETs. Therefore, TFETs represent an attractive alternative to MOSFETs towards low voltage operations and power consumption.

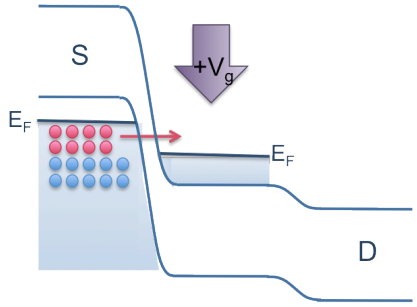

Fig. 1.5 Carrier transport through the barrier in BTBT FETs

1.4. Research Objective and Outlines

Fig. 1.6 shows the basic lateral PIN structure of a TFET, and its turn-on mechanism. The applied gate bias causes the bend bending by modulating the electrical fields in the channel. At the sufficient band bending, the distance between the valence and conductions bands is short enough to allow the quantum mechanical tunneling of electrons.

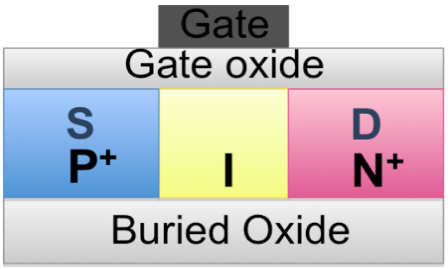

(a)

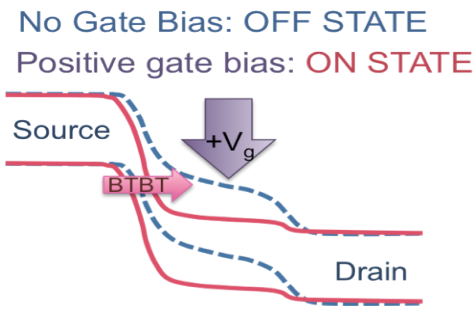

(b)

Fig. 1.6 (a) The structure of a lateral PIN TFET (b) A band diagram illustrating the turn-on of the device by band-to-band tunneling of electrons

However, a sharp source-channel interface and an excellent channel electrostatic control through the gate contact are two key issues in TFETs to obtain a high ON-current and a low SS. These two properties are rather difficult to obtain, especially in lateral p-i-n structures where the source contact is often etched away and regrown. Contrary to lateral TFETs, BTBT diodes with a vertically grown p-n interface can be easily fabricated and offer a very good opportunity to test the tunneling properties of a given material and its potential as a tunneling transistor.

A thorough investigation of the underlying physics of BTBT diodes will help understanding the TFET operation, and assist the analysis of TFET design. Therefore, in this thesis, homogeneous InGaAs p-n tunneling diodes lattice matched to InP is investigated using a full-band and atomistic quantum transport approach based on the tight-binding model. This thesis also presents the necessary high doping effects such as band gap narrowing, and the physical phenomena such as excess current, which affect the performance of the device. The physical based device simulator OMEN is used to illustrate the effectiveness of theses approaches, and the simulation results are compared to experimental data of Penn State University and Notre Dame University where possible.

The remainder of the thesis is composed of three chapters. In chapter 2, the basic concepts of a BTBT diode and its current-voltage characteristics are described. The basic physics and calculation method of band gap narrowing is presented in chapter 3, and the results obtained by simulation are compared with experiment data and discussed in chapter 4. In chapter 5, the conclusion and future plan for the research are briefly introduced.

2. BAND-TO-BAND TUNNELING DIODES

2.1. Introduction

A Band-to-band tunneling (BTBT) diode, also referred as an Esaki diode, is the semiconductor device based on quantum mechanical tunneling. Due to the wave nature of carriers, they can leak through the energy barrier of higher energy.

A BTBT diode consists of degenerate p^+-n^+ layers with very high impurity concentrations in both sides and a sharp transition at the junction.

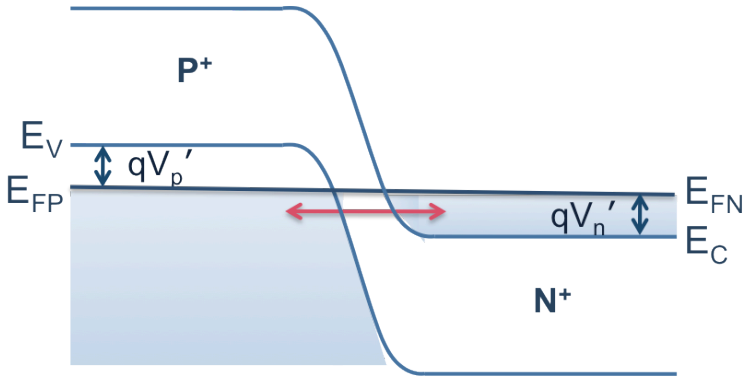

Fig. 2.1 Schematic energy band diagram of a BTBT diode in thermal equilibrium

Fig. 2.1 shows the schematic energy band diagram of a BTBT diode at zero bias, and the direction of carrier flow represented by a red arrow. Fermi levels (E_{FP}, E_{FN}) are located within the allowed bands due to the heavy dopings, and the amount of degeneracy (V_p', V_n') is typically a few kT/q. Depletion layer width is typically less than 10 nm, which is considerably narrower than the conventional p-n junction. [5]

A BTBT diode has a very short transit time due to the tunneling of majority carriers while traditional transistors and diodes have slow transit time, which depends on the diffusion velocity of minority carriers. Therefore, a BTBT diode is capable of very fast operation because current changes rapidly with the voltage change. With this possibility of operation at very high frequencies, a BTBT diode can be used as an oscillator and a high-frequency threshold (trigger) device. However, a BTBT diode has been replaced by other semiconductor devices because it is difficult to fabricate due to its abrupt and high doping profiles. Also, semiconductor devices such as a Gunn diode and an IMPATT diode have surpassed its performance, and for many purposes, a three-terminal device, such as a field-effect transistor, is more flexible than a device with only two terminals.[5] Yet, investigating the properties of a BTBT diode is still important to test the fundamental tunneling properties of a given material and its potential as a tunneling transistor.

It is important to review the underlying physics of the device to understand the implications of modeling and analysis of the device performance. Therefore, in this chapter, the basic physics and behavior of a BTBT diode will be introduced.

2.2. Basic Physics of Tunneling

In classical physics, the electrons cannot pass the potential energy barrier unless they have the energy higher than the barrier. However, in quantum mechanics, electrons are described by the wavefunctions, and the attenuation wave with an imaginary k value represents the electrons in the barrier. Therefore, the electrons with the energy lower than the barrier can tunnel through the barrier as described in Fig. 2.2 with the finite tunneling probability, which is expressed as [6]

$$P_t \approx \frac{16E(U-E)}{U^2}\exp\left(-2W\sqrt{\frac{2m}{\hbar^2}(U-E)}\right) \tag{2.1}$$

The above equation shows that the height and the width of the potential barrier as well as electron mass are key parameters, which determine the tunneling probability. There is more possibility of tunneling for the narrower and smaller energy barrier, and lighter electrons. This relationship can be applied to any shape of potential barrier problem.

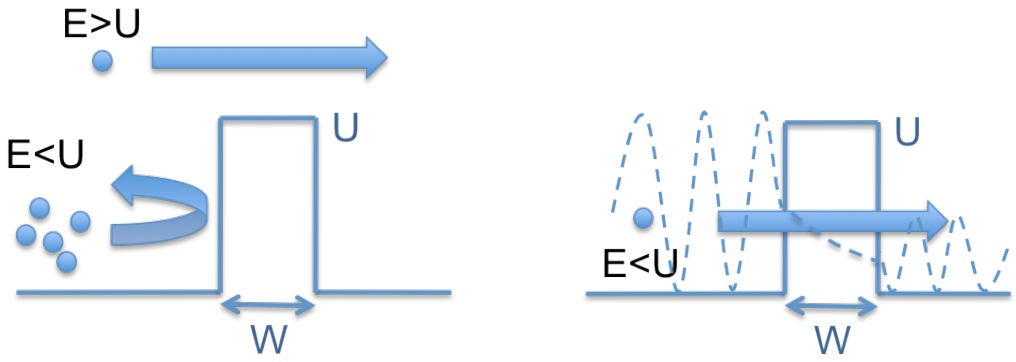

(a) (b)

Fig. 2.2 (a) Semi-classical, and (b) quantum mechanical descriptions of the electrons movement when they face the energy barrier

For BTBT, the electrons tunnel through the triangular shaped energy barrier from valence band to conduction band as shown in Fig. 2.3. Since these electrons have very low energy, BTBT is not affected by the thermal distribution of carriers, which limits SS. This inter-band tunneling has a finite probability when the electric field in a semiconductor is sufficiently high, on the order of 10^6V/cm.

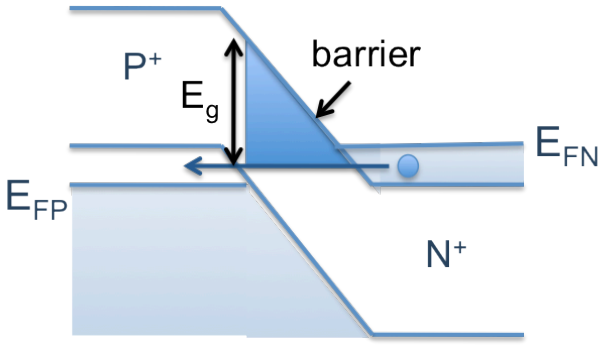

Fig. 2.3 Triangular shaped energy barrier and tunneling of carriers in a BTBT diode

The BTBT probability for direct tunneling through the triangular barrier with uniform field, ε, can be calculated using WKB (Wentzel-Kramers-Brillouin) approximation [7]:

$$P_t \approx \exp\left(-\frac{4\sqrt{2m^*}E_g^{3/2}}{3q\hbar\varepsilon}\right) \tag{2.2}$$

In the equation, all kinetic energies are assumed to be in the direction of tunneling. High tunneling probability is expected for small effective mass and small band gap energy. Large electric field will also lead to high tunneling probability as it causes the sharp junction with a narrower barrier width.

2.3. Current-Voltage Characteristics

In a conventional p-n diode, the device is conducted when the junction is forward biased (where p-side has positive bias with respect to n-side), and the current is blocked at the reverse biases up to the breakdown voltage where large current, which usually destroy the device starts to flow. On the contrary, a BTBT diode can be conducted under reverse bias where the breakdown voltage is zero due to the heavy doping of the device. However, when forward biased, an odd effect called negative differential resistance (NDR) occurs where the forward current decreases with the increase of the voltage. NDR implies that the amount of tunneling current in a BTBT diode depends on the size of a tunneling window, which is the energy range where the available energy state on one side and the empty states on the other side of the diode overlap. These current-voltage characteristics of a BTBT diode are illustrated in Fig. 2.4.

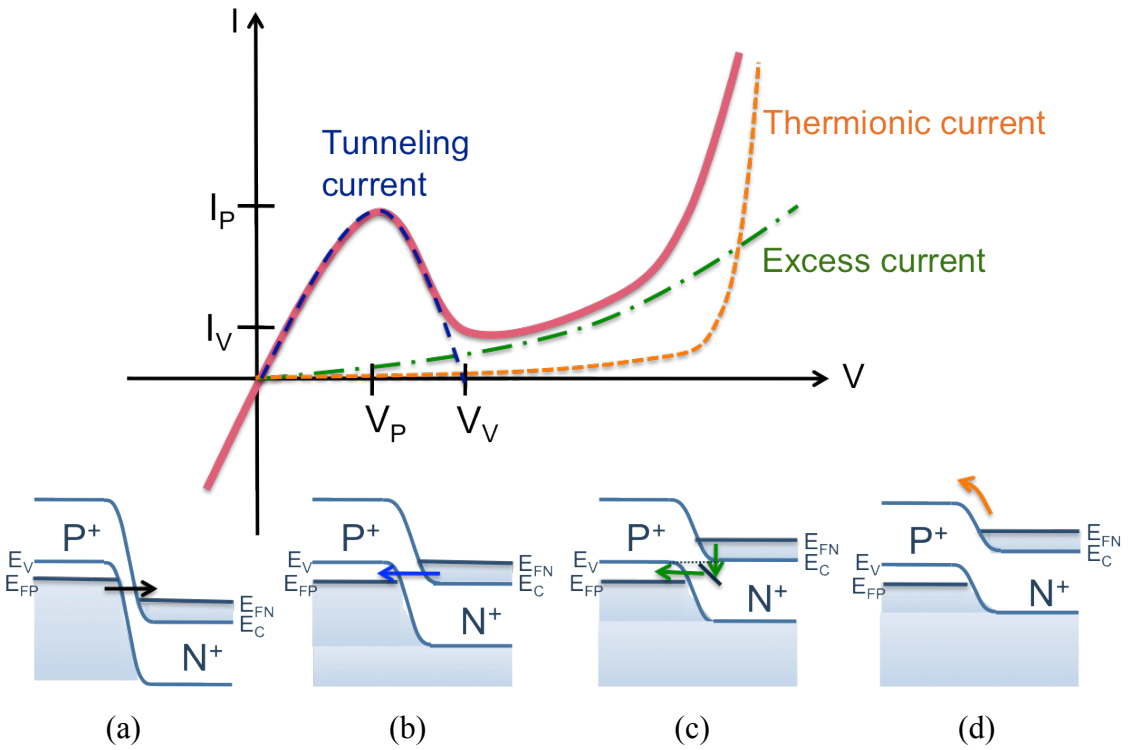

Fig. 2.4 Static current-voltage characteristics of a BTBT diode including its three current components, and the corresponding energy band diagrams

There is a monotonically increasing tunneling current in reverse-direction while the forward-biased current consists of the three components: band-to-band tunneling current, excess current, and thermionic current (also referred as diffusion or thermal current).[8] In Fig. 2.4, each energy band diagram shows the current dependence on the band alignment; (a) When a reverse bias is applied, there are filled states on the p-side and unoccupied states on the n-side. Then, electrons in the p-type valence band can tunnel into the n-type conduction band. The increase of a reverse voltage gives a wider tunneling window, and therefore monotonically increasing tunneling current. (b) For a forward-biased device, on the other hand, the forward current flows due to the inter-band tunneling of electrons from the n-side to the p-side until the bands are uncrossed. The peak current (I_P), the maximum forward tunneling current, flows when the tunneling window is maximized where the most of the electrons in the n-side and most of available states in the p-side have the same energy and are right opposite to each other. (c) At the

point where the bands are uncrossed ($V=V_p'+V_n'$), the bottom of the n-type conduction band (E_C) and the top of the p-type valence band (E_V) are aligned at the same energy, and tunneling current cannot flow any more since there are no empty states opposite to the filled states. However, the valley current (I_V), the minimum forward current, has a non-zero value due to the excess current. An excess current flows due to the tunneling of electrons through the gap states. (d) With the further forward voltage increase, the excess current and normal thermionic currents are dominated, and current increases exponentially with the voltage.

2.3.1. Tunneling Current

Tunneling current is a major current component of a BTBT diode at both of the reverse and the low forward biases. In these bias ranges, the inter-band tunneling of electrons between conduction and valence bands occurs when the certain conditions are met: (1) There are occupied energy states on the one side. (2) There are empty states on the opposite side at the same energy levels with the filled states that electrons can tunnel through. (3) The potential barrier has a low height and a small width that there is a finite tunneling probability of electrons. (4) The momentum is conserved in the tunneling process.[9]

From the condition (4), we can expect that there are two ways to conserve the momentum in tunneling processes: direct and indirect tunneling. Direct tunneling occurs when the electrons tunnel from the conduction band minimum (E_c) to the valence band maximum (E_v) without changing momentum in k-space. Therefore, it can happen in the direct semiconductors where E_c and E_v have the same k-value (Γ-point). Direct tunneling also could be placed in indirect semiconductor if there is sufficiently large applied voltage that electrons can tunnel from higher conduction band valley to E_v. In indirect semiconductor, on the other hand, indirect tunneling also can occur. In this case, there should be scattering processes by phonons or impurities to conserve the momentum. In general, the indirect tunneling has much lower probability than the direct tunneling when both of the tunneling processes are possible.[10]

The tunneling current under forward bias can be calculated from the equation 2.3.[11]

$$I_t = C\int [F_C(E) - F_V(E)]P_t N_C(E)N_v(E)dE \tag{2.3}$$

C is a constant, $F_C(E)$ and $F_V(E)$ are the Fermi-Dirac distribution functions, and $N_C(E)$ and $N_V(E)$ are the density of states in the conduction and valence bands, respectively. However, it is difficult to get an analytical solution of the equation 2.3. Instead, the following empirical formula can be used to calculate tunneling current under forward bias.[9]

$$I_t \simeq \frac{I_P V}{V_P}\exp(1-\frac{V}{V_P}) \tag{2.4}$$

where

$$V_P = \frac{V_p' + V_n'}{3} \tag{2.5}$$

The equations show that at the higher doping where V_n' and V_p' increase, the peak voltage (V_P) shifts to a higher value and the tunneling current (I_t) increases.

2.3.2. Excess Current

A high BTBT current flows across the junction at low forward biases. In an ideal BTBT diode, this tunneling current decreases to zero when the applied forward voltage exceed V_n'+V_p', where the energy bands are uncrossed. Therefore, for sufficiently high biases, energy-conserving inter-band tunneling of electrons are no longer possible and only the normal diode current should flow by forward injection of minority carriers. However, in practice, the current between such biases is unexpectedly in excess of the normal diode current. This current is called the excess current.[12]

There are two possible mechanisms leading to excess current. In the first case where gap states are ignored, electrons should dissipate their energy during the tunneling by emitting photons, phonons, plasmons, or in Auger processes. Kane[13] considered these hypotheses in a theoretical point of view, and concluded that theses effects are too small to explain the excess currents. Kane also suggested the other possible mechanism as a source of excess current, which is originally suggested by Yajima and Esaki[14]: the most excess currents are associated with the tunneling of carriers via energy states in the forbidden gap, which are mostly originated from the band edge tails. In a heavily doped

semiconductor, the random distribution of charged impurities cause potential fluctuations of the band edges, which result in the tailed off density of states into the forbidden gap as illustrated in Fig. 2.5[15]. Also, these localized energy states in the forbidden gap can be introduced during the junction fabrication process, or by imperfection such as dislocations.[13]

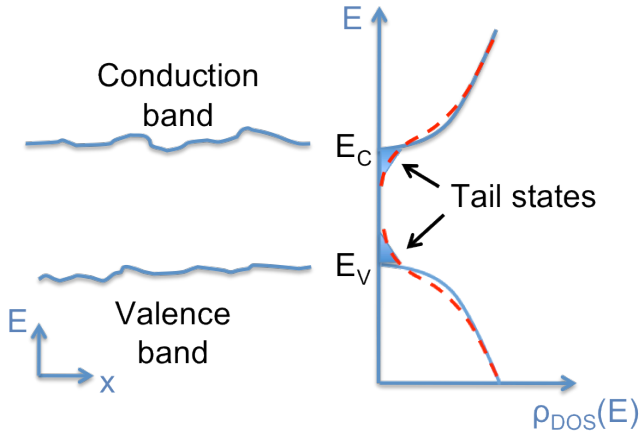

Fig. 2.5 Spatial fluctuation of band edges due to the random distribution of impurities, and band edge tails in a heavily doped semiconductors[15]

Chynoweth et al. [12] suggested the possible mechanism of excess current based on the suggestion of Esaki, and explained the exponential nature of this current.

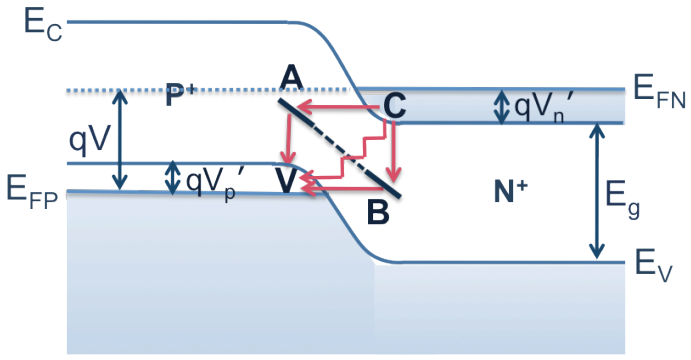

Fig. 2.6 Tunneling mechanisms via states in the forbidden gap in the excess current bias range[12]

Fig. 2.6 illustrates some possible routes of electrons from the states in the n-type conduction band (C) to the p-type valence band (V) in the forward bias range where the excess current is dominant. The states A and B represent the local energy levels in the forbidden gap, which are most likely tails of acceptor levels and donor levels extending to the forbidden gap, respectively. An electron at C can drop down to an empty level at B, then directly tunnel to V. Similarly, an electron also can tunnel from C to another local state A from which it then drops down to V. Another possible route is CABV where an electron dissipates its excess energy at the impurity-band conduction between A and B. For the last, there can be staircase route from C to V. This is a series of tunneling and energy-loss processes of an electron between local levels, and possible when there are sufficiently high numbers of energy states in the forbidden gap. The route CBV is regarded as the basic mechanism.

Based on this basic mechanism, the excess current is proposed with the following equation.[12]

$$\ln I_x = \ln C_1 + \ln D_x - C_2\{E_g - qV + q(V_n' + V_p')\} \tag{2.6}$$

C_1 and C_2 are constants, and D_x is the volume density of the occupied levels at B above E_v. The equation predicts the exponential increase of the excess current with the applied forward bias where $qV \ll E_g$, and can be rewritten in the form of

$$\ln I_x = \ln I_v + C_3(V - V_v) \tag{2.7}$$

where C_3 is a constant, and I_v and V_v are the current and the voltage at the valley.[14] Excess current is observed at the current range between the valley (I_v) and the thermionic current where the bias exceeds half the band gap.

2.3.3. Thermionic Current

At large forward biases, the familiar thermionic current by a flow of minority carriers over the junction barrier is dominant. This current is normal forward diode current, which follows the rectifier equation,

$$I_d = I_0[\exp(\frac{qV}{akT}) - 1] \tag{2.8}$$

where I_0 is a saturation current, and $1 \le a \le 2$ in most common cases.

2.3.4. Summary

The complete static current-voltage equation for a BTBT diode under forward bias can be expressed as

$$I = I_t + I_x + I_d \simeq \frac{I_P V}{V_P}\exp\left[1-\frac{V}{V_P}\right] + I_V \exp\left[C_3(V-V_V)\right] + I_0\left[\exp\left(\frac{qV}{kT}\right)-1\right] \tag{2.9}$$

Each current component dominates in different bias range. The tunneling current (I_t) and thermionic or diffusion current (I_d) are dominant at the voltage below and above V_v, respectively. The excess current, I_x, has a significant contribution at the voltages around V_v. [17]

Since the maximum forward current (I_p) is a part of the tunneling current, it depends on the junction abruptness, while the minimum forward current (I_v) depends on the distribution and concentration of energy levels in the forbidden gap. Therefore, high peak-to-valley ratio I_p/I_v can be obtained by planar processes such as MBE and MOCVD. These techniques yield higher and sharper doping profiles for higher I_p, as well as lower defect densities for lower I_v. [18]

Both of the excess and thermionic currents have an exponential I-V characteristic, but they can be distinguished from each other by their different dependence on temperature. The excess current is nearly temperature-independent, and therefore can be clearly seen in the low temperature characteristics. In some diodes with very low excess current, the exponential increase of excess current can be found at the voltages just below the onset of the thermionic current, or is not observed at all. [19]

3. BAND GAP NARROWING EFFECT

3.1. Basic Concepts of Band Gap Narrowing Effect

The band gap energy of semiconductors is one very important parameter in the modeling of device properties since it determines the electrical and optical behaviors of the devices. From the equation 2.2 in chapter 2, it is clear that the band gap of the material plays a significant role in BTBT current. At heavily-doped semiconductors, typically with the doping levels above $10^{18}/cm^3$ for most III-V semiconductors, the density of energy states depends on the impurity concentrations. The impurity states overlap and form an impurity band as shown in Fig. 3.1. Also, the random distribution of impurities causes the potential fluctuation of the band edges, and impurity states tails into the forbidden gap as described in Fig. 2.5 in chapter 2.3.2.[20] As the result of the broadening of impurity band and the formation of band tails into the forbidden gap, the band gap energy decreases as much as 200meV with the increase of impurity concentration.[21] This effect is usually referred to as band gap narrowing (BGN).

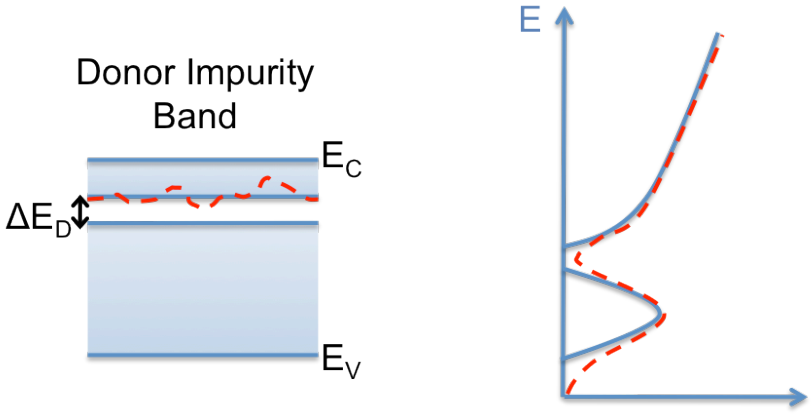

Fig. 3.1 The donor impurity band formation in a heavily doped n-type semiconductor for the ordered (solid line), and randomly distributed (dashed line) impurities[20]

The many-body interactions provide more reasonable explanation on the causes of the BGN. Due to the interaction energy between free carriers and between free carriers and ionized impurities, the conduction band edge can be lowered or the valence band edge can be raised. The main energy contributions in n- and p-type semiconductors are [22]: (1) Electron-electron interaction. The spin interaction energy and the Coulombic interaction result in a net attractive energy and a decrease in the conduction band edge. (2) Electron-donor interaction is attractive and leads to lowering of the conduction band edge. (3) Hole-hole interaction. The spin interaction energy and the Coulombic interaction result in a net attractive energy and an increase in the valence band edge. (4) Hole-acceptor interations is attractive and leads to an increase of the valence band edge. (5) Electron-hole interaction in highly excited semiconductors. Such interactions result in a net band gap reduction and become important at small carrier-to-carrier distances. Therefore, BGN occurs in heavily-doped semiconductors as well as in undoped, but highly excited semiconductors with high free carrier concentrations.[22]

In BTBT diodes, current mainly flows through the p-n junction either by tunneling or thermionic emission, and depends on the size of energy barrier. BGN disturbs this energy barrier by altering the distribution of energy between conduction and valence bands. Therefore, BGN should be considered in such a device where both sides of layers are heavily-doped, since it significantly influences current through the junction and the device performance.

3.2. Calculation of Band Gap Narrowing

3.2.1. Introduction

There have been a number of theories based on various approaches about calculation of BGN. Classical theories based on Thomas Fermi screening do not predict the BGN correctly, and a quantum mechanical description is required. Mahan[23] wrote a theoretical paper based on the many-body theory, in which he postulated five possible energy contributions for the band shifts, and calculated the BGN in n-Si and n-Ge as a function of impurity concentration. Berggren and Sernelius[24] suggested physically more accurate model for the band shifts based on second order perturbation theory and

Random Phase Approximation (RPA) calculations for screening. There is another approach to calculate band shifts known as Plasmon Pole Approximation (PPA)[25, 26], which simplifies the complex calculation of RPA. These methods provide physically accurate, but very complex numerical calculations, which is not suitable for device simulation.

Therefore, many commercial device simulators calculate BGN by the simple empirical logarithmic models of Slotboom[21] and del Alamo[27] or usually ignore this effect. However, these models do not have any physical meaning, and they need experimental fitting parameters. Also, due to the lack of the experiment data of BGN of materials other than Si, Ge, and GaAs, they cannot provide the correct calculation for other materials. Additionally, in most cases in calculating BGN, it is considered that the whole band gap reduction occurs only in the majority carrier band or is split evenly between both bands. However, since the partitioning of the total BGN between the valence and conduction bands determines the form and size of energy barrier, this approach can lead to incorrect results. Therefore, a general phenomenological expression, which is capable of calculating each band shift separately as a function of doping concentration for all material is needed.

3.2.2. Compact Model of Band Gap Narrowing Based on Many-body Effects[28-30]

Jain and Roulston suggested a closed form analytical expression for BGN based on Mahan's approach. Theoretically, their approach is less rigorous than full RPA calculation but useful for CAD analysis in that it is in a very simple form and capable of calculating band shifts in major and minor bands separately for all materials.

In their theory, the equations for band shifts are derived by identifying the 4 contributions to BGN: shift of the majority band edge due to exchange energy ($\Delta E_{ex(maj)}$), correlation energy shift of the minority band edge ($\Delta E_{cor(mino)}$), and carrier-impurity interaction shifts of the two band edges ($\Delta E_{int(maj)}$, and $\Delta E_{int(mino)}$). The shifts $\Delta E_{ex(maj)}$ and $\Delta E_{cor(mino)}$ are called many-body shifts, and the total BGN (ΔE_g) can be obtained by adding all these shifts.

$$\Delta E_g = \Delta E_{ex(maj)} + \Delta E_{cor(mino)} + \Delta E_{int(maj)} + \Delta E_{int(mino)} \quad (3.1)$$

Adding all these energy contributions, Jain and Roulston obtained a simple expression for the BGN applicable to all semiconductors as a function of doping concentration (N). Also, there are no fitting parameters in this equation, and the BGN is only the function of R and r_s, which depend on the material parameters such as the effective masses of carriers and dielectric constant.

$$\frac{\Delta E_g}{R} = 1.83 \frac{\Lambda}{N_b^{1/3}} \frac{1}{r_s} + \frac{0.95}{r_s^{3/4}} + [1 + \frac{R_{(\text{mino})}}{R}] \frac{1.57}{N_b r_s^{3/2}} \tag{3.2}$$

Here, R and $R_{(\text{mino})}$ are the effective Rydberg energy for majority and minority bands, respectively, and r_s is the average distance between majority carriers, normalized to the effective Bohr radius.

$$R = \frac{m^* e^3}{8\varepsilon^2 h^2} [eV] \tag{3.3}$$

$$R_{(\text{mino})} = \frac{m^*_{(\text{mino})} e^3}{8\varepsilon^2 h^2} [eV] \tag{3.4}$$

$$r_s = \frac{r_a}{a} \tag{3.5}$$

where

$$r_a = \left(\frac{3}{4\pi N} \right)^{1/3} \tag{3.6}$$

$$a = \frac{4\pi\varepsilon\hbar^2}{m^* e^2} \tag{3.7}$$

e is an electron charge, ε is a permittivity of a semiconductor, h is a Plank constant, N_b is the number of equivalent band extrema, m* and m_{min}* are majority and minority carrier density of state effective masses, respectively. Λ and N_b are correction factors, which account for anisotropy of the n-type semiconductor bands, interaction between the heavy- and light-hole bands in p-type semiconductors, and distortion due to heavy doping. These parameters have a unity values if the bands are parabolic and isotropic. By their assumptions, Λ=0.75, N_b=2 for all p-type semiconductors, Λ=1 and the average of the heavy hole and the light hole masses are used for m_{min}* in n-type semiconductors for the high doping range between $10^{18}/cm^3$ and $10^{20}/cm^3$. This model is successfully applied

to n-Si, p-Si, n-Ge, p-GaAs and p-GaSb, with the results in close agreement with full RPA calculation and the published experiment data.

The equation (3.2) can be expressed as a function of the impurity concentration (N) where A, B, and C are the constants which can be calculated from the material parameters.

$$\Delta E_g = AN^{1/3} + BN^{1/4} + CN^{1/2} \tag{3.8}$$

This equation can be divided and rewritten into majority and minority band shifts (ΔE_{maj} and ΔE_{mino}, respectively) of the following equations where C_1, C_2, C_3, and C_4 are the constants.

$$\Delta E_{\text{maj}} = C_1\left(\frac{N}{10^{18}}\right)^{1/3} + C_2\left(\frac{N}{10^{18}}\right)^{1/2} \tag{3.9}$$

$$\Delta E_{\text{mino}} = C_3\left(\frac{N}{10^{18}}\right)^{1/4} + C_4\left(\frac{N}{10^{18}}\right)^{1/2} \tag{3.10}$$

For p-type semiconductor, the majority band shift due to an increase of E_v, and the minority band shift due to the lowering of E_c are denoted by ΔE_v and ΔE_c, respectively.

$$\Delta E_v = \frac{0.125}{\varepsilon_r}\left(\frac{N}{10^{18}}\right)^{1/3} + \frac{0.0084}{(\varepsilon_r m_{dh})^{0.5}}\left(\frac{N}{10^{18}}\right)^{1/2} \tag{3.11}$$

$$\Delta E_c = \frac{0.3628 m_{dh}^{0.25}}{\varepsilon_r^{1.25}}\left(\frac{N}{10^{18}}\right)^{1/4} + \frac{0.0084 m_{de}}{\varepsilon_r^{0.5} m_{dh}^{1.5}}\left(\frac{N}{10^{18}}\right)^{1/2} \tag{3.12}$$

For n-type semiconductor, the majority and minority band shifts are ΔE_c and ΔE_v, respectively.

$$\Delta E_c = \frac{0.21}{\varepsilon_r}\left(\frac{N}{10^{18}}\right)^{1/3} + \frac{0.0168}{(\varepsilon_r m_{de})^{0.5}}\left(\frac{N}{10^{18}}\right)^{1/2} \tag{3.13}$$

$$\Delta E_v = \frac{0.3628 m_{de}^{0.25}}{\varepsilon_r^{1.25}}\left(\frac{N}{10^{18}}\right)^{1/4} + \frac{0.0084(m_{hh} + m_{lh})}{\varepsilon_r^{0.5} m_{de}^{1.5}}\left(\frac{N}{10^{18}}\right)^{1/2} \tag{3.14}$$

(*note: Appendix A - Band shifts by Jain-Roulston BGN model)

4. HOMO-JUNCTION INGAAS BAND-TO-BAND TUNNELING DIODES

4.1. Introduction

From the previous equations in chapter 2, it is obvious that the performance of a BTBT diode is affected by the BTBT probability, which depends on the effective mass and band gap energy of the material exponentially. Since the smaller values of these two material parameters increase the BTBT probability, the interest on the base material of this device has moved from Si to Ge, and to the III-V direct semiconductor materials with smaller band gap and effective mass, such as InAs. The parameters of theses materials as well as the ones of $In_{0.53}Ga_{0.47}As$ are compared in Table 4.1. $In_{0.53}Ga_{0.47}As$, which is a base material of the considered devices in this research, is also a direct III-V semiconductor material with a relatively low electron effective mass, and a small energy band gap. $In_{0.53}Ga_{0.47}As$ also offers an advantage in fabrication process in that it is lattice matched to InP, which can be used for the substrate material. These properties make $In_{0.53}Ga_{0.47}As$ a good candidate for the tunneling device.

Table 4.1 Band gap energy and electron density of state effective mass of various materials at 300K

Materials	E_g [eV]	m_e^*/m_0
Si	1.12	1.08
Ge	0.67	0.55
InAs	0.35	0.023
$In_{0.53}Ga_{0.47}As$	0.75	0.041

In BTBT diodes where both sides of layers are heavily-doped, simple parabolic band approximation is no longer available since this is only an accurate approximation near the band edges. At highly doped semiconductors where the donor concentration (N_D) and the

acceptor concentration (N_A) become comparable or greater than the conduction band density of state (N_C) and the valence band density of state (N_V), respectively, the carrier energy is significantly higher than the band minima, and the density of states depends on the impurity concentration. In most commercial simulators, a simple parabolic band model is used regardless of high N_D, and N_A. This yields the Fermi level, E_f, deeper into the conduction or valence bands. Also, the industrial standard, the drift-diffusion model, augmented by a simple tunneling model such as the WKB or Kane's approach require considerable user customization, and is not accurate enough to treat tunneling devices whose behaviors are dominated by quantum mechanical effects. Therefore, in this thesis, homogeneous $In_{0.53}Ga_{0.47}As$ BTBT diodes are examined by a full-band and atomistic quantum transport approach based on the tight-binding model.

This chapter examines the performance of the $In_{0.53}Ga_{0.47}As$ BTBT diodes fabricated in Penn State University (Case 1) and Notre Dame University (Case 2), the partners in the MIND center. Simulations and experimental data of the devices are compared where possible.

4.2. Methodology and Simulation Environment

Based on the fabricated $In_{0.53}Ga_{0.47}As$ BTBT diodes, one-dimensional structures are constructed on numerical simulation. To investigate the I-V characteristics of the devices, OMEN, a full-band, atomistic quantum transport simulator based on the tight-binding model and the Non-equilibrium Green's Function (NEGF) formalism[31] is used. The sp3d5s* tight-binding model with spin-orbit coupling is used for the ballistic simulation at 300K.

The exact BGN at each band edge of the n- and p- sides of the diodes are calculated as a function of their doping concentrations by Jain-Roulston model[26] since any experimental data of $In_{0.53}Ga_{0.47}As$ have not been reported. Since the Jain-Roulston model successfully interpreted experiment data of BGN for p-type III-V materials such as GaAs and GaSb, it is expected that their BGN parameters for p-$In_{0.53}Ga_{0.47}As$[28] will reasonably estimate BGN. However, for the heavily-doped n-type III-V semiconductors, this model seems to need some corrections.[30] This model is based on the rigid band model that the parameters Λ=1, and N_b=1 of n-type III-V semiconductors do not count

the nonparabolicity and sub-bands effects of the conduction band, which cannot be neglected at highly doped n-type III-V semiconductors. Therefore, in this thesis, numerically fitted parameters[31] are used for n-type $In_{0.53}Ga_{0.47}As$.

Since the Jain-Roulston model is a function of R and r_s, which depend on effective masses of carriers and dielectric constant of the material, the parameters of the equation 3.8 for $In_{0.53}Ga_{0.47}As$ can be also expected to have the values between those of InAs and GaAs. Therefore, the BGN parameters of n-$In_{0.53}Ga_{0.47}As$ are estimated by linear interpolation between the parameters of InAs and GaAs. For this estimation, the published BGN parameters[30], which showed the agreement with the published experiment data are used for n-GaAs. The BGN parameters used for InAs are extracted from a least squares fit to the experimental data at the N_D level of $2\times10^{17}/cm^3$ to $2\times10^{18}/cm^3$[31].

The BGN parameters in Table A.2, and A.3 in the appendix A are used for the calculation of total BGN of p-type and n-type $In_{0.53}Ga_{0.47}As$, respectively. These parameters are recalculated into the form of the equation 3.9 and the equation 3.10 to calculate the each band shift separately, and those new parameters for band shifts are summarized in Table A.4 in the appendix A. Fig. 4.1 shows the calculated total BGN as well as each band shift as a function of doping concentration for n- and p- type $In_{0.53}Ga_{0.47}As$.

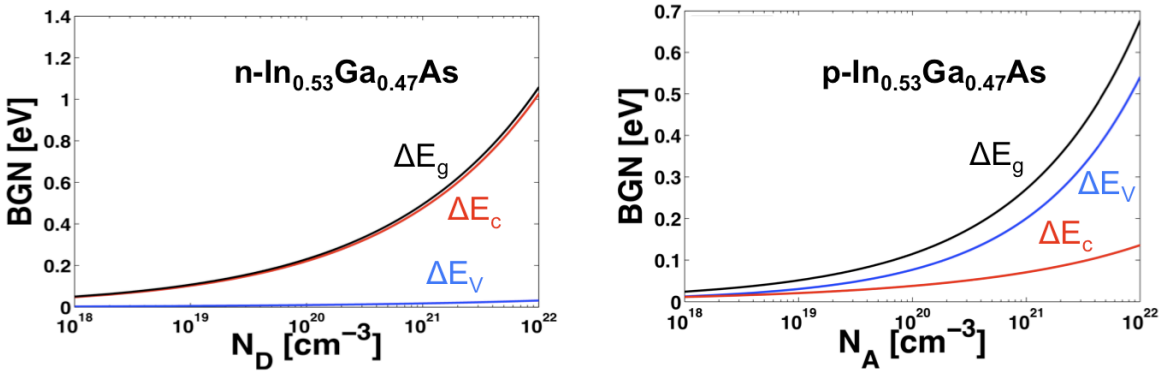

Fig. 4.1 Calculated total BGN and band shifts as a function of doping concentration for n- (left) and p- type (right) $In_{0.53}Ga_{0.47}As$

In Fig. 4.1, n- and p-type $In_{0.53}Ga_{0.47}As$ show about 200meV, and 150meV of the total BGN, respectively, at the typical doping range of BTBT devices ($10^{18}/cm^3$ to $10^{19}/cm^3$). The total BGN of n-$In_{0.53}Ga_{0.47}As$ is almost twice more than the one of p-$In_{0.53}Ga_{0.47}As$ unlike Si and Ge where there is more BGN in p-type. This is mostly because $In_{0.53}Ga_{0.47}As$ has a single conduction valley, which reduces the parameter N_b, and therefore the total BGN. For the both of n- and p-type $In_{0.53}Ga_{0.47}As$, most BGN occurs in the majority bands. However, in n-type material, the shift of minority band is much smaller than the one of p-type material due to the smaller electron mass compared to the hole mass.

The impact of BGN is implemented in the quantum transport simulation by modifying the tight binding-parameters of $In_{0.53}Ga_{0.47}As$ for each side of the diode. The effective band gap, which is reduced by the amount of the total BGN is calculated for n- and p- sides of the device. Then, from these reduced band gap values, new Indium and Gallium compositions (1-x and x, respectively), which result in theses reduced band gap are calculated by the equation 4.1.

$$E_g = 0.43x^2 + 0.63x + 0.36 \tag{4.1}$$

The equation 4.1 describes the compositional dependence of the band gap of $In_{1-x}Ga_xAs$ at Γ-point at 300K. The tight-binding parameters of each side is recalculated from their x values by linearly interpolating the parameters of InAs and GaAs and adding a Bowing parameter. Then, by shifting the diagonal energy to the band edges of both sides, the complete tight-binding parameters for $In_{1-x}Ga_xAs$ with the reduced band gap for each layer are obtained. Fig. 4.2 illustrates this process.

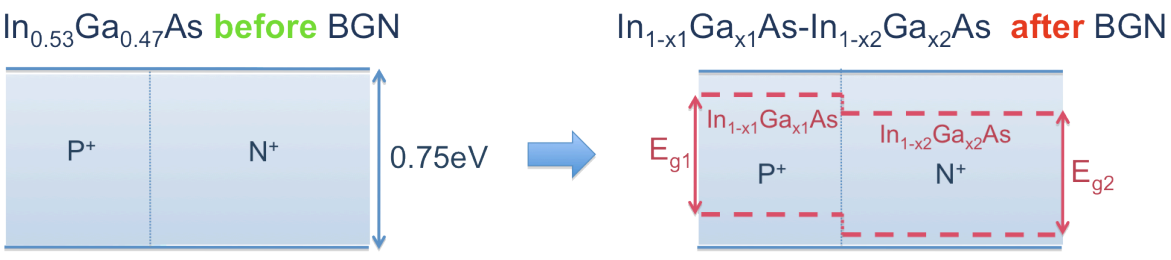

Fig. 4.2 Illustration of including BGN effect in the simulation

In Fig. 4.2, when BGN is applied, p- and n- sides of the diode have the different Indium and Gallium compositions ($In_{1-x1}Ga_{x1}As$, and $In_{1-x2}Ga_{x2}As$, respectively) with the corresponding band gaps (E_{g1} and E_{g2}, respectively) since they have different doping type and concentration. The resulted structure in the figure is hetero-structure like, and the spatial variation in the effective alloy concentration x mimic the band gap narrowing. All other material parameters such as lattice constant, and dielectric constant keep the same values with $In_{0.53}Ga_{0.47}As$.

4.3. Reproducing and Understanding Experimental Data: Case 1

4.3.1. Experimental Structure and Data

A homo-junction BTBT diode consist of InGaAs lattice matched to InP is fabricated by the group of Suman Datta in Penn State University, a partner in the MIND center. Fig. 4.3 shows the schematic view, and measured I-V data at various temperatures of the BTBT diode with a 600nm radius.

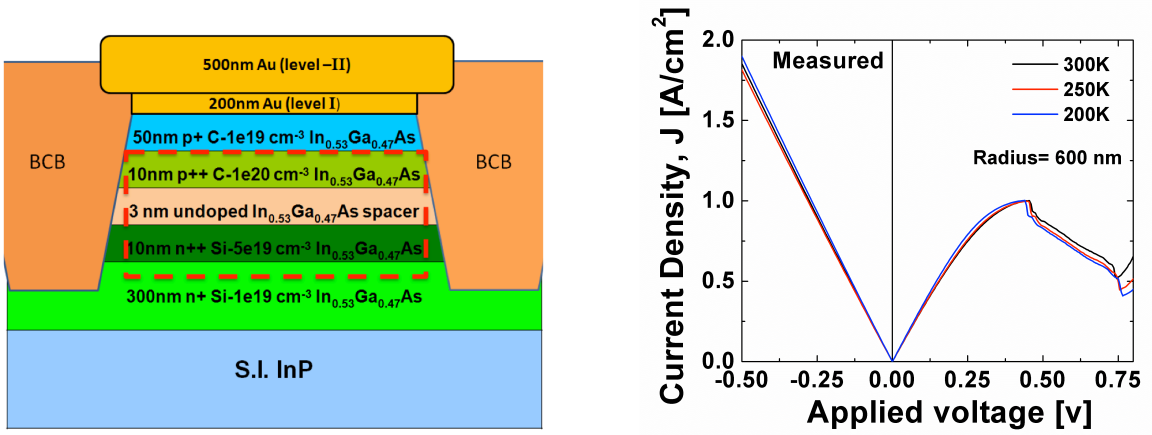

Fig. 4.3 Schematic diagram of a fabricated $In_{0.53}Ga_{0.47}As$ homo-junction BTBT diode, and measured I-V characteristics of the device

The peak current of the device measured 1MA/cm^2, and the experimentally estimated series resistance value is 20 Ω.

4.3.2. Modeling and Simulation Approach

The red dotted region in Fig. 4.3 set as the simulation domain, and the representative structure is shown in Fig. 4.4.

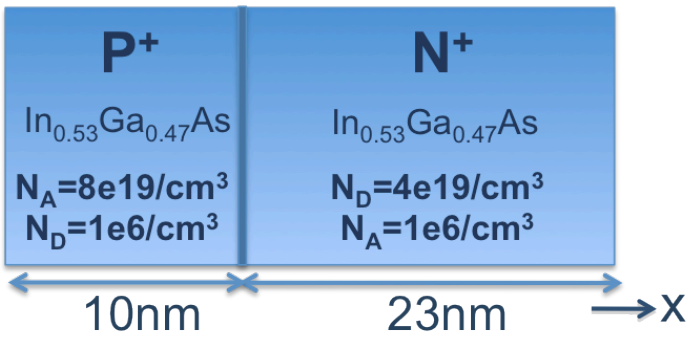

Fig. 4.4 The one-dimensional BTBT diode structure and doping profiles used in the simulation

Fig. 4.4 represents the one-dimensional $In_{0.53}Ga_{0.47}As$ BTBT diode structure constructed in OMEN. In the simulation, 3nm intrinsic layer between p- and n-sides of the device is ignored, and the step-junction with constant doping profiles on both sides is used to demonstrate the abrupt transition of heavy doping at the junction.

The doping profile at the junction determines the magnitude of the electric field in the device, and affects the amount of the tunneling currents. Fig. 4.5 shows the influence of doping abruptness at the junction on the Zener tunneling current (reverse-biased side tunneling current) of the device. The simulation results for a step junction and a graded junction are compared with the experiment data. The structure with the step junction is expected to provide more tunneling current than linearly graded junction since it has the energy barrier with a smaller width, which yields smaller electric field.

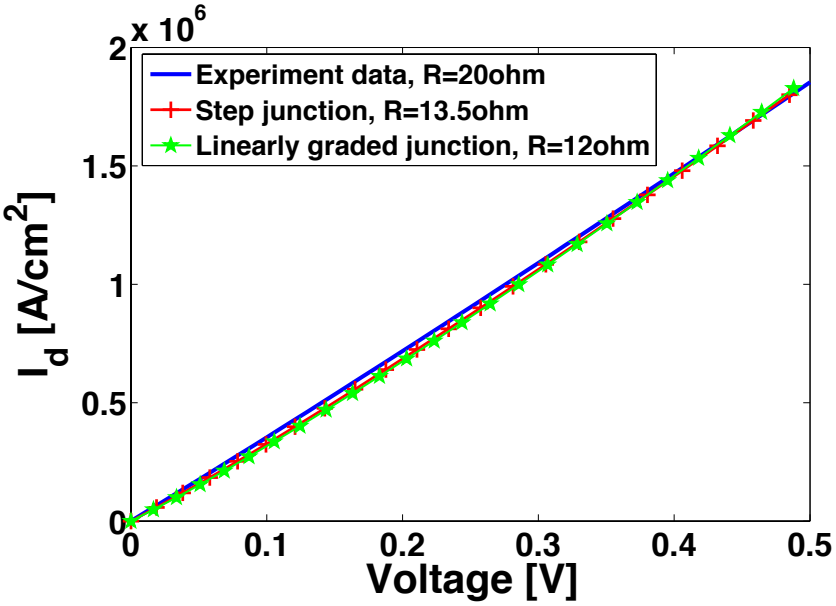

Fig. 4.5 The influence of p-n junction doping profiles on the Zener tunneling current

In Fig. 4.5, the series resistances are calculated in a way to match the simulation data to the experiment data. The fitted series resistance value of the device with step junction (13.5 Ω) is closer to the experimentally estimated value of 20 Ω, but still far from the expected value. This small series resistance implies that the simulated current is smaller than the measured Zener current, and that there should be some physical meaning of correction to increase the tunneling current. As discussed in the previous chapters, band gap scaling can be one possible approach to increase the diode current.

Fig. 4.6 compares the experimental data at 300K of Fig. 4.3 with the simulated results of two different InGaAs devices under forward biases. The two simulated devices have the same dimension and doping densities as described in Fig. 4.4, but different compositions of Indium and Gallium. All the data in Fig. 4.6 is corrected for series resistances matched to the Zener current.

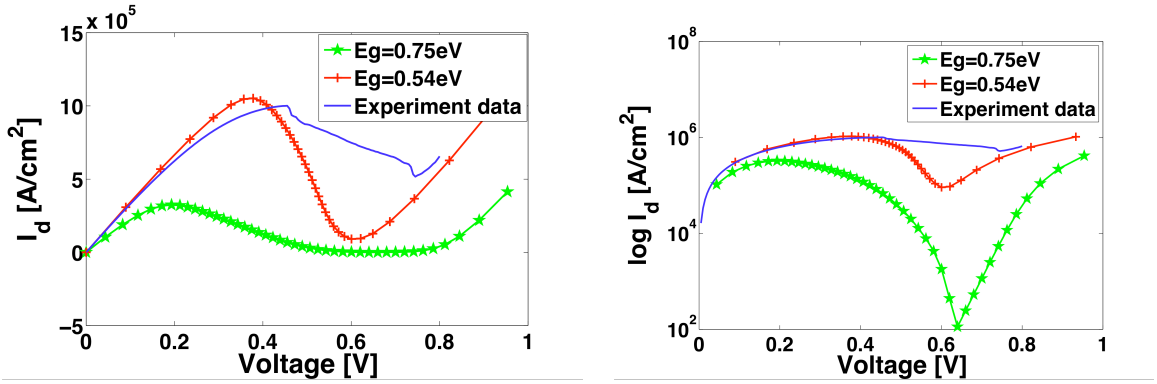

Fig. 4.6 The influence of small band gap on the device current under forward biases

In Fig. 4.6, the blue line shows the experimental data of $In_{0.53}Ga_{0.47}As$ device, and the green and red lines show the simulation data of the devices with $In_{0.53}Ga_{0.47}As$ and $In_{0.75}Ga_{0.25}As$, respectively. Typically, as we have seen in Fig. 4.1, heavily-doped III-V semiconductors at the doping levels around $10^{18}/cm^3$~$10^{19}/cm^3$ have about 200meV band gap reduction. Therefore, $In_{0.75}Ga_{0.25}As$ with a band gap about 200meV less than the one of $In_{0.53}Ga_{0.47}As$ is used to anticipate the BGN effect on the device current. The device with 75% of Indium, which has a smaller band gap, shows a good agreement with the experimental data except for the NDR region while the simulated $In_{0.53}Ga_{0.47}As$ diode provides much lower forward current and onset of the thermionic current at the larger bias. This result suggests that BGN effect plays an important role in the determination of the current peak and the turn-on point of the thermionic current.

However, as discussed in chapter 3, BGN is a function of doping concentration and splits into the conduction and valence bands unevenly. Therefore, each band shifts for both of the n- and p-sides of the device should be correctly calculated to examine the effect of BGN on the performance of the device. Fig. 4.7 illustrates each band shift calculation using Jain-Roulston model, and Fig. 4.8 shows the importance of this calculation. The amount of majority and minority band shifts as well as the total BGN calculated by the Jain-Roulston model and the parameters in Table A.4 in the appendix A are summarized in Table. 4.2.

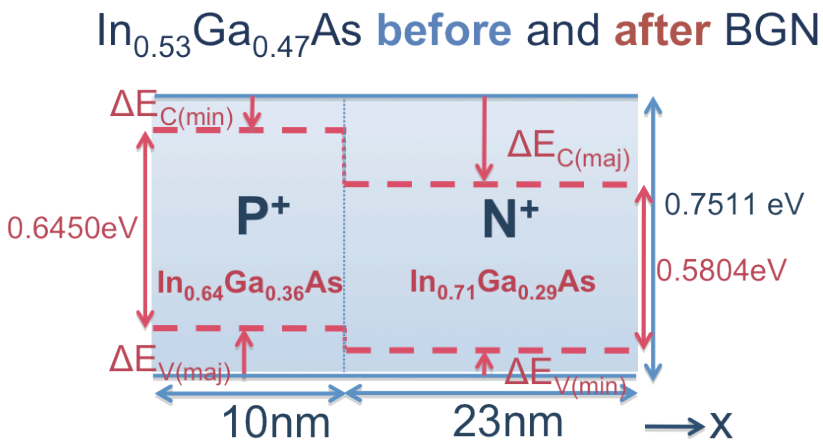

Fig. 4.7 The band shifts and the effect of BGN on the device

Table 4.2 Calculated band shifts and total BGN of the device at doping of $N_A=8\times10^{19}/cm^3$ and $N_D=4\times10^{19}/cm^3$

Energy Band Shift [eV]	Source (P^+)	Drain (N^+)
$\Delta E_{maj}=\Delta E_{ex}+\Delta E_{int}$	$\Delta E_V=0.0702$	$\Delta E_C=0.1628$
$\Delta E_{mino}=\Delta E_{cor}+\Delta E_{int}$	$\Delta E_C=0.0358$	$\Delta E_V=0.0079$
$\Delta E_G=\Delta E_{maj}+\Delta E_{mino}$	$\Delta E_G=0.1061$	$\Delta E_G=0.1707$

The resulted structure with BGN in Fig. 4.7 is hetero-structure like, composed of $In_{0.64}Ga_{0.36}As$ and $In_{0.71}Ga_{0.29}As$ on p- and n-sides, respectively, with different band gaps. In order to see the importance of the calculation of each band shifts, the simulated current of this structure is compared with the simulated results of two other cases: the total BGN distribution in a majority band only, and 50:50 distribution of the total BGN between conduction and valence bands. Fig. 4.8 shows the result of this comparison, and it is clearly seen in the figure that the distribution of the total BGN determines the current peak and the turn-on point of the thermionic current. Therefore, the exact calculation of each band shift is needed to get the accurate I-V characteristics of the device.

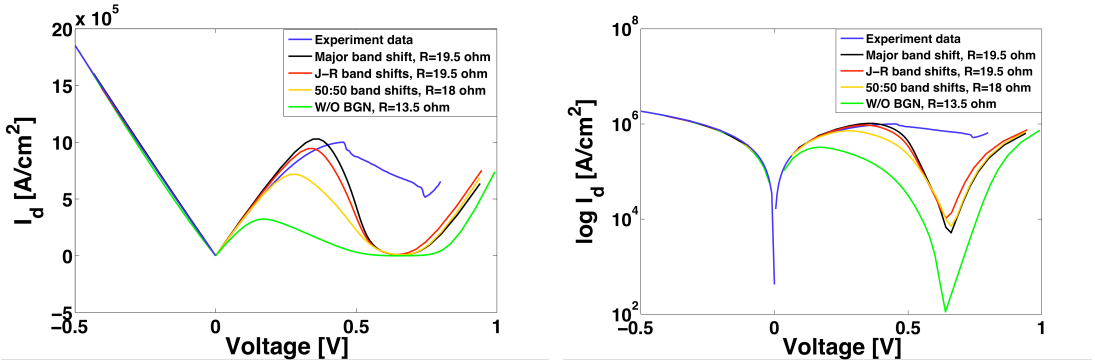

Fig. 4.8 The importance of exact band shift calculation

4.3.3. Results and Discussion: BGN Effect

Fig. 4.9 shows the current-voltage characteristics of the considered device. The simulated current of the device with BGN (red line) is compared with the simulation data in an absence of the BGN (green line), and the experimental data (blue line). The Zener tunneling currents of the simulated data are matched to the experimental curve with different values of series resistances.

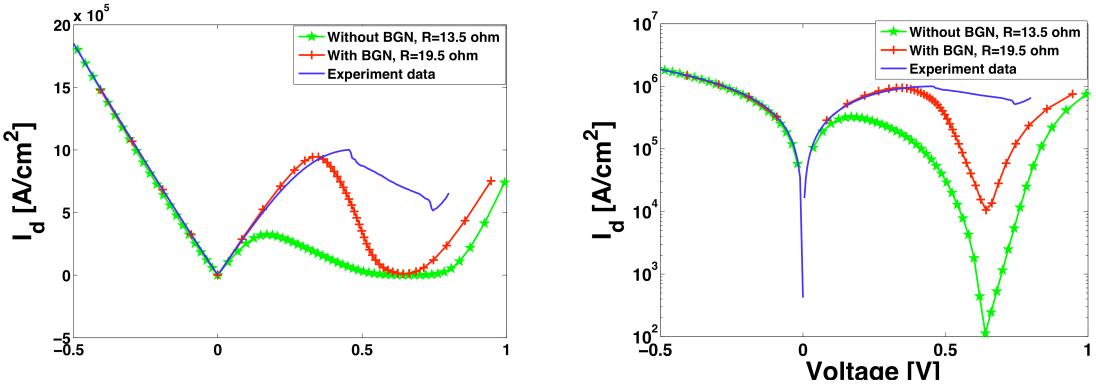

Fig. 4.9 BGN effect on I-V characteristics of the device

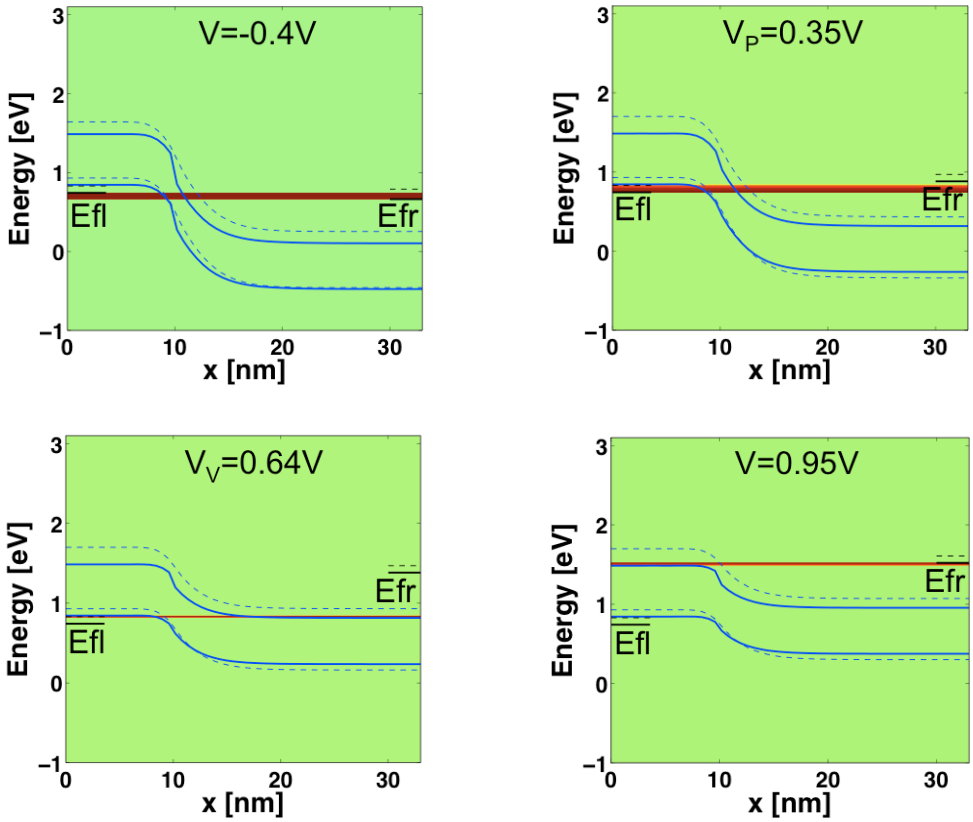

Fig. 4.10 The current flow and the corresponding band diagrams of the structure including BGN (solid line). The band diagrams of the structure without BGN are also shown with the dotted lines

Fig. 4.10 shows the current flow of the device including BGN at various bias points, and the corresponding band diagrams (solid line) are compared with the band diagrams of the device without BGN (dotted line) to demonstrate the effect of BGN. Each figure represents the Zener tunneling current, the peak current, the valley current, and the thermionic current in clockwise direction starting from the upper left diagram, and the Fermi levels of the left contact and the right contact are denoted by Efl and Efr, respectively. The black solid lines are the Fermi levels of the structure including BGN, and the black dotted lines are the Fermi levels of the structure without BGN.

In Fig. 4.9, experimental Zener tunneling branch of the considered diode is relatively well reproduced by the simulation approach when BGN is included. The matched series resistance for this case (19.5 Ω) agrees with the experimentally extimated value of 20 Ω

while the matched value of the device without BGN provides much lower value of 13.5 Ω. It can be also expected from the upper left picture in Fig.4.10 that when BGN is not included, the tunneling window is smaller, and therefore less Zener tunneling current will flow at -0.4V.

On the other hand, noticeable differences for the forward biased side are observed in Fig. 4.9 when BGN is included: (i) the peak current is significantly closer to the experimental data (ii) the simulated current in the NDR region is too small, (iii) an earlier turn-on of the thermionic current, but still occurs at too large bias. The first feature is the result of the reduced band gap, which increases the tunneling current. While the underestimation of the valley current can be explained by the absence of electron-phonon scattering in the simulation model, convincing explanation for the third point is needed. Assuming that a doping extracted from SIMS (Secondary ion mass spectrometry) measurement can be different with the ideal doping profile used in the simulation, investigating the influence of impurity concentration on the onset of thermionic current will be a good approach to this issue.

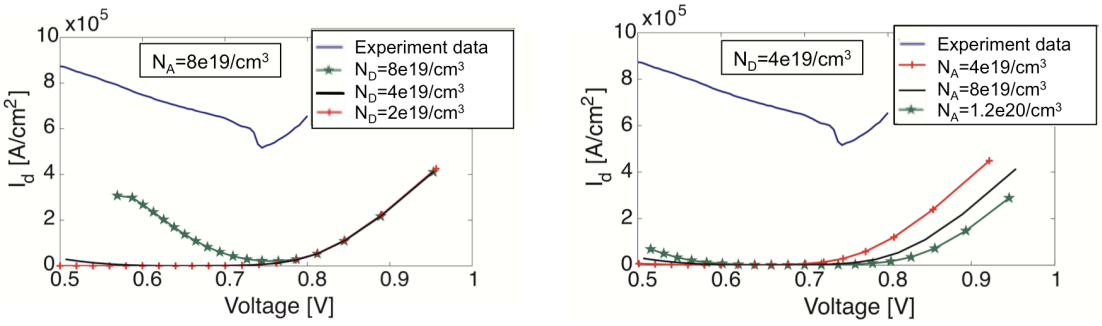

Fig. 4.11 The influence of (a) donor, and (b) acceptor concentrations on the onset of the thermionic current

The left-hand side and the right-hand side pictures of Fig. 4.11 show the current change around the valley point due to the variation of the donor (N_D) and the acceptor (N_A) concentrations, respectively. The change of N_D does not affect the on-set of the

thermionic current while the decrease of N_A leads to the earlier turn-on of the thermionic current. This can be explained with the band diagrams in Fig. 4.12.

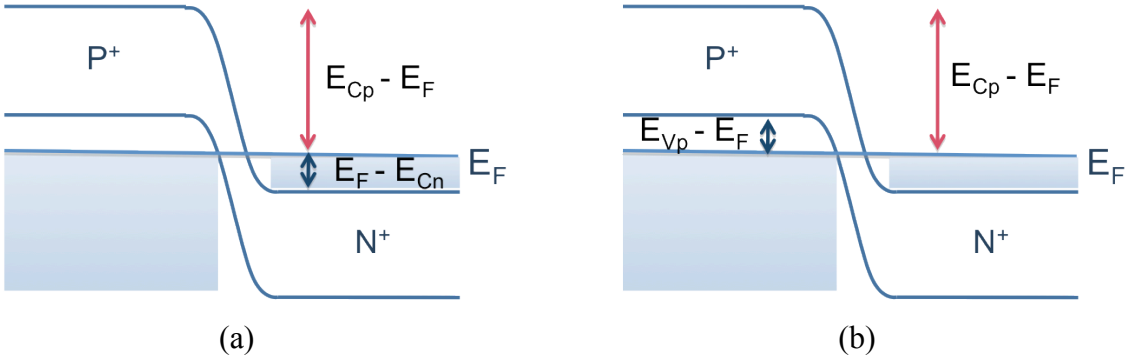

Fig. 4.12 The band diagrams illustrating the effects of (a) donor, and (b) acceptor concentrations on the current around the valley

The most thermionic current is due to the flow of electrons over the energy barrier from n-side to p-side. Therefore, the shift of the conduction band edge of p-side determines the onset of the thermionic current since it changes the potential barrier height. The variation of N_D effects on the value of E_F-E_{Cn}, but not on the height of the junction barrier, E_{Cp}-E_F, in Fig. 4.12 (a) where E_F is a Fermi level, and E_{Cn} and E_{Cp} are conduction band edges of n- and p-sides, respectively. The increase of N_D increases the value of E_F-E_{Cn} by lowering the n-side conduction band edge, and this yields the increase of forward tunneling current. On the other hand, the variation of N_A makes the change of E_{Cp}-E_F value, and therefore affects the junction barrier height in Fig. 4.12 (b). The decrease of N_A reduces the value of E_{Cp}-E_F by lowering p-side conduction band edge, and therefore results in the earlier turn-on of the thermionic current. Also, the increase of N_A increases E_{Vp}-E_F, which, in turn, more forward tunneling current. However, since the band shifts of p-type are much smaller than the n-type, these effects due to the variation of N_A are very small as shown in Fig. 4.11.

The change of the peak and thermionic currents can be also expected when we compare the simulated structure in Fig. 4.7 with the $In_{0.75}Ga_{0.25}As$ diode used in Fig. 4.6. The band gaps of p- and n- sides of the $In_{0.53}Ga_{0.47}As$ device with BGN are about 0.65eV

and 0.58eV, respectively, and both values are larger than the band gap of $In_{0.75}Ga_{0.25}As$ (0.54eV). However, the difference between the n-conduction band edge and p-valence band edge (0.5525eV) has the almost same value with the band gap of $In_{0.75}Ga_{0.25}As$. Therefore, we can approximately compare those two structures as illustrated in Fig. 4.13.

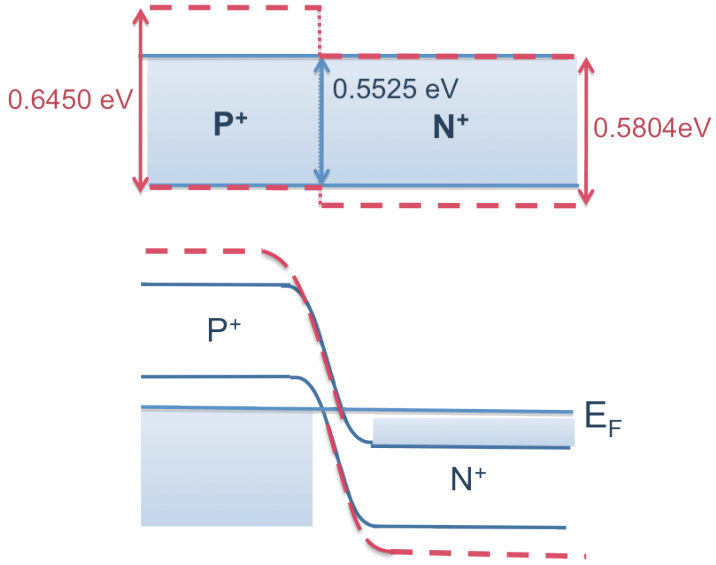

Fig. 4.13 The schematic comparison between the simulated structures composed of $In_{0.75}Ga_{0.25}As$ (solid line) and $In_{0.53}Ga_{0.47}As$ with BGN (dotted line)

In Fig. 4.13, it is assumed that the location of the Fermi levels of both devices is the same. Therefore, the tunneling windows of both structures are the same, which, in turn, there is the same amount of the tunneling current for both devices. However, since the $In_{0.53}Ga_{0.47}As$ device with BGN has the higher potential barrier for the electrons, the thermionic current will start to flow at the higher bias. It can be seen from Fig. 4.6 and Fig.4.9 that the peak currents of those two devices are almost the same while there is a shift of the thermionic current in $In_{0.53}Ga_{0.47}As$ device with BGN.

4.3.4. Results and Discussion: Excess Current

In the previous discussion with the results of Fig. 4.12, it was found that there is not so much change on the onset of the thermionic current in the reasonable doping range. Purely ballistic NEGF calculations seem to be not enough to model BTBT diodes due to missing device physics, and we need to see this problem in a different point of view: there is an excess current above the valley in the experimental data compared to the simulated current at the same bias range. This excess current can be interpreted by the current through the gap states, which is described in chapter 2.

If we assume that there are enough gap states introduced during the junction fabrication process, we should be able to find the exponential excess current at the bias right above the valley. Fig. 4.14 shows the raw data of the current of the considered device. Simulation data are not fixed with any series resistances, and the experimentally estimated value of 20 Ω is extracted from the experiment data. The slopes of the current starting from the valley are shown with the dotted lines in the figure.

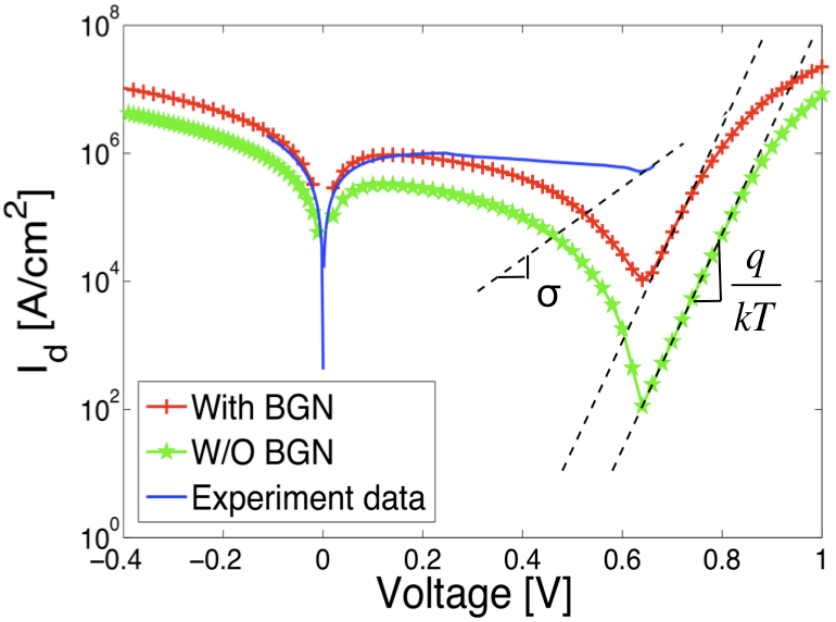

Fig. 4.14 The intrinsic I-V characteristics of the device

The thermionic current follows the rectifier equation 2.8 of a normal diode that it can be presented by a line of slope close to q/kT in a semi-logarithmic plot. The slopes of simulated currents in the bias range exceeding the valley point show this dependence whether they include BGN effect or not. Even though there is not enough experimental data beyond the valley, it is clear that there exists an exponential current with much lower slope (almost 1/3.2 of q/kT), and few orders of magnitude higher than the conventional diode current. This lower slope verifies the existence of the excess current at the bias range where the slope is measured. Furthermore, this semi-logarithmic plot implies that there must be a more or less continuous distribution of states inside the forbidden gap as we assumed at the beginning of this approach.

Once we verify the existence of the excess current, we can calculate this current from the equation 2.7, which can be rewritten in the form of

$$I_x = I_v \exp(\sigma(V - (V_v - I_v R_s)) \tag{4.2}$$

Here, I_v and V_v are current and voltage at the valley, respectively, and R_s is a series resistance. Assuming that the excess current is dominant at the valley, the slope of experimental data at the valley is used for the constant σ. The measured values of those parameters from the experimental data are listed in Table 4.3.

Table 4.3 The measured parameters for the excess current calculation

I_v [A/cm^2]	V_v [V]	R_s [Ω•cm^2]	σ
5.164×10^5	0.745	$20(600\times10^{-7})^2\pi$	12.1

From the equation 4.2, and the parameters in Table 4.3, the excess current included in the experimental data are calculated. Figure 4.15 shows this calculated excess current.

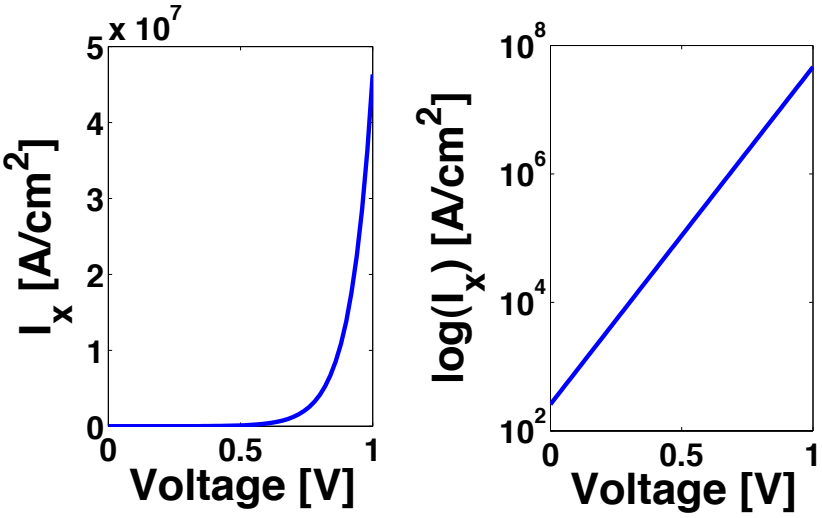

Fig. 4.15 The calculated excess current from the experimental data

Fig. 4.15 shows the exponential nature of the excess current, which is dominant at the bias range beyond the valley. This calculated excess current is added to the intrinsic simulated current. Fig. 4.16 illustrates the added excess current, and Fig. 4.16 shows the effect of this approach.

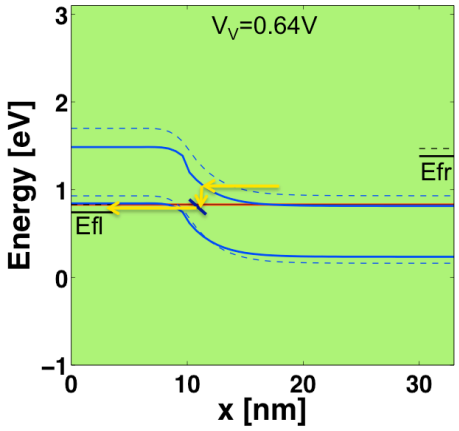

Fig. 4.16 The excess current (yellow arrows) should be added to the valley current

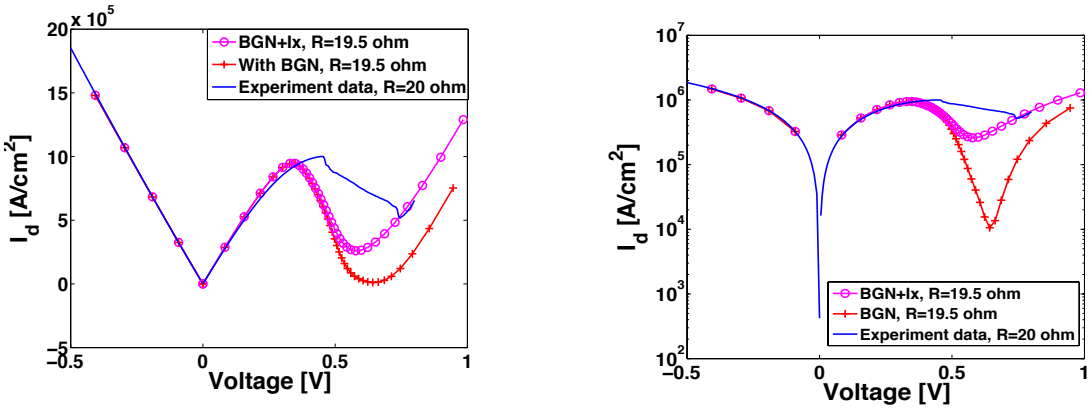

Fig. 4.17 The effect of the excess current on the device current when BGN is considered

Fig. 4.17 shows the effect of the excess current on the I-V characteristics of the device including BGN. The exponential excess current added to the ballistic simulated data increases the current around and beyond the valley close to the experimental curve.

On the other hand, by adding the excess current to the simulated current without BGN, we can reexamine the effect of BGN on the I-V characteristics of the device as shown in Fig. 4.18.

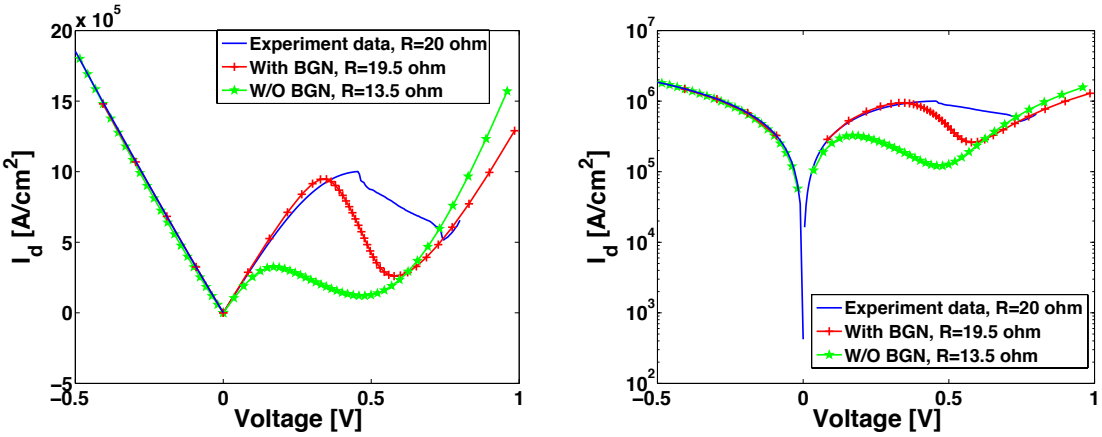

Fig. 4.18 The effect of BGN on the I-V characteristics of the device when the excess current is considered

Fig. 4.18 demonstrates the effect of the BGN on diode current when the excess current is included. The result clearly shows that the BGN significantly increases the tunneling currents on the both of the positive and the negative bias regions.

4.3.5. Results and Discussion: Temperature

The high density theories on which Jain-Roulston model is based are strictly valid only at very low temperatures. At room temperature, there could be 0 to 20 meV more BGN.[28] Fig 4.19 shows the effect of the increased BGN at room temperature on the device current under forward bias. 20 meV increase of the total BGN is assumed, and this value is split into conduction and valence bands with the same ratio of their original shifts. The increase of BGN yields the slightly higher peak current, but does not influence the onset of the thermionic current.

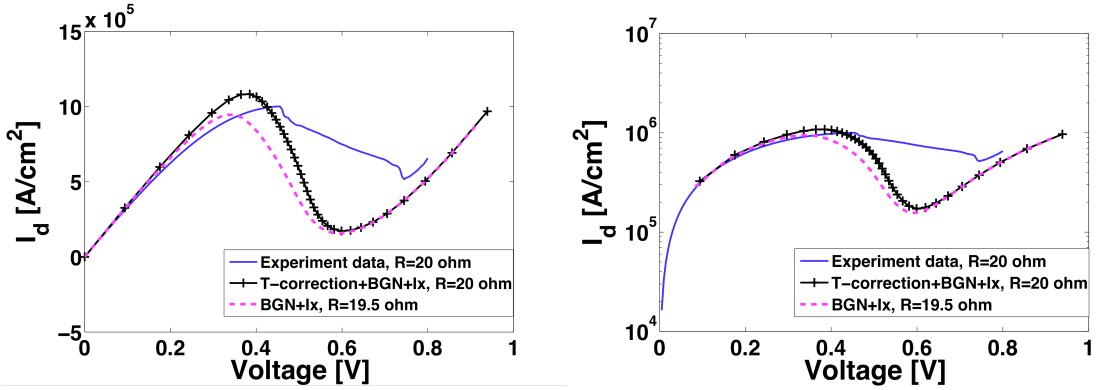

Fig. 4.19 The effect of temperature on the I-V characteristics under forward bias

4.4. Reproducing and Understanding Experimental Data: Case 2

4.4.1. Experimental Structure

A homo-junction BTBT diode consist of InGaAs lattice matched to InP is fabricated by the group of Alan Seabaugh in Notre Dame University, a partner in the MIND center. Fig. 4.20 shows the schematic view of the BTBT diode with the ideal doping profiles.

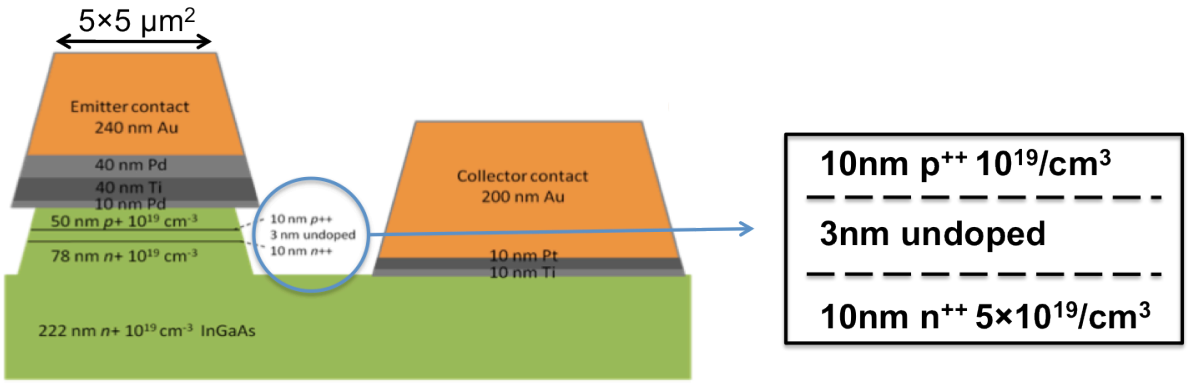

Fig. 4.20 Schematic diagram of a fabricated $In_{0.53}Ga_{0.47}As$ homo-junction BTBT diode

4.4.2. Modeling and Approach of the Simulation

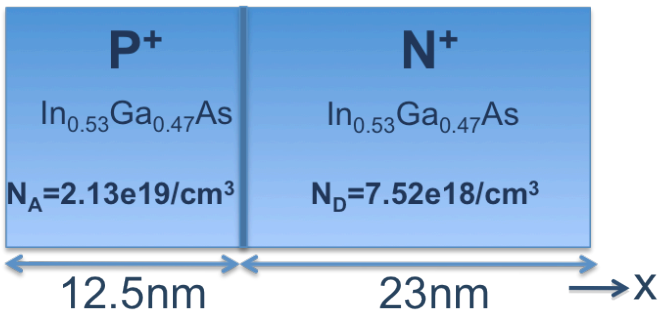

Fig. 4.21 The one-dimensional BTBT diode structure and doping profiles used in the simulation

Fig. 4.21 represents the one-dimensional $In_{0.53}Ga_{0.47}As$ BTBT diode structure constructed in OMEN. In the simulation, 3nm intrinsic layer between p- and n-sides of the device is ignored, and the doping extracted from SIMS measurement is used. The doping levels described in Fig. 4.20 are the maximum values of the SIMS data, which are used for BGN calculation.

Fig. 4.22 illustrates each band shift and the effect of BGN on the device. The resulted structure with BGN is hetero-structure like, composed of $In_{0.6}Ga_{0.4}As$ and $In_{0.63}Ga_{0.37}As$ with different band gaps. The amount of majority and minority band shifts

as well as the total BGN calculated using the Jain-Roulston model and parameters in the Table A.4 in the appendix A are summarized in Table. 4.4.

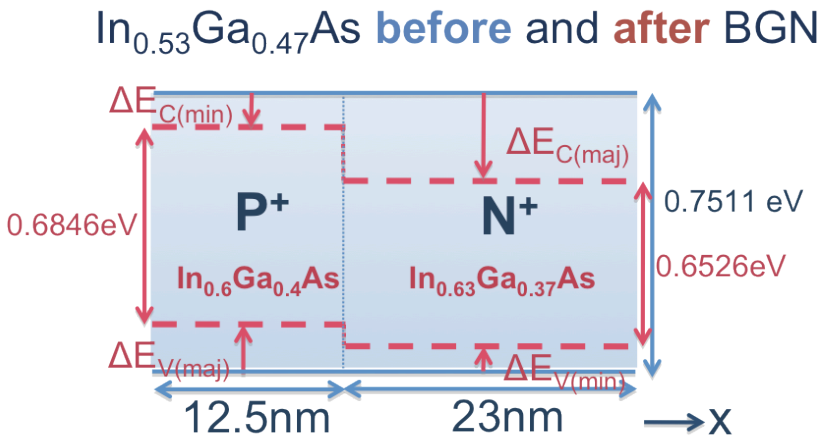

Fig. 4.22 The band shifts and the effect of BGN on the device

Table 4.4 Calculated band shifts and total BGN of the device at doping of $N_A=2.13\times10^{19}/cm^3$ and $N_D=7.52\times10^{18}/cm^3$

Energy Band Shift [eV]	Source (N^+)	Drain (P^+)
$\Delta E_{maj}=\Delta E_{ex}+\Delta E_{int}$	$\Delta E_C=0.0933$	$\Delta E_V=0.0412$
$\Delta E_{mino}=\Delta E_{cor}+\Delta E_{int}$	$\Delta E_V=0.0052$	$\Delta E_C=0.0253$
$\Delta E_G=\Delta E_{maj}+\Delta E_{mino}$	$\Delta E_G=0.0985$	$\Delta E_G=0.0665$

4.4.3. Simulation Results and Discussion: BGN Effect

Fig. 4.23 shows the current-voltage characteristics of the device. The simulated current of the device with BGN (red line) is compared with the simulation data in an absence of the BGN (green line), and the experimental data (blue line). The Zener tunneling currents of the simulated data are matched to the experimental curve with different values of series resistances.

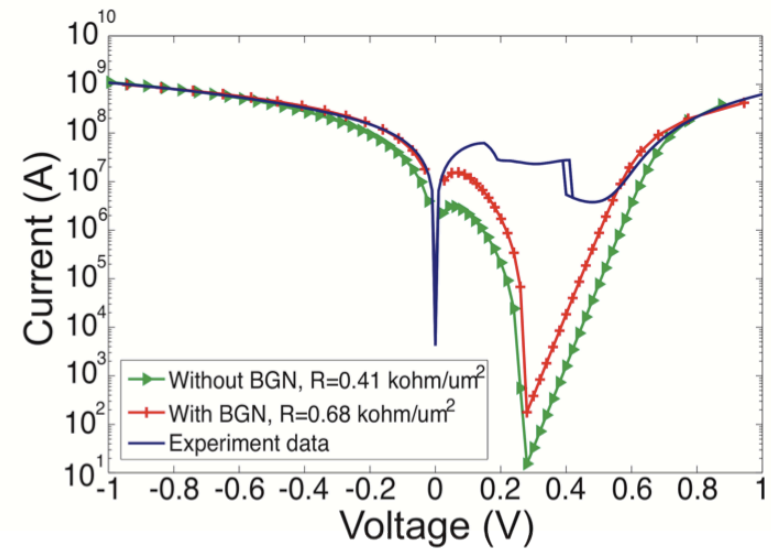

Fig. 4.23 BGN effect on I-V characteristics of the device

Fig. 4.23 shows that experimental Zener tunneling branch of the considered diodes are relatively well reproduced by the simulation approach, and the peak current is increased when BGN is applied. Low valley current can be explained by the absence of electron-phonon scattering in the simulation model. However, there are too much current for Zener tunneling side while there is not enough increase for the peak current. Therefore, to match the experimental data on the Zener tunneling side, the series resistance (R_S) values larger than 0.35 kΩ/μm^2, which is measured from the experiment data are used.

From the results of Fig. 4.11, it can be expected that higher donor concentration and more acceptor doping will increase the forward tunneling current including the peak current. The effect of high donor and acceptor concentrations when BGN is included is shown in Fig. 4.24. The constant doping profiles are used for both cases, and they are compared with the experiment data, and the simulated current with the doping extracted from SIMS measurement.

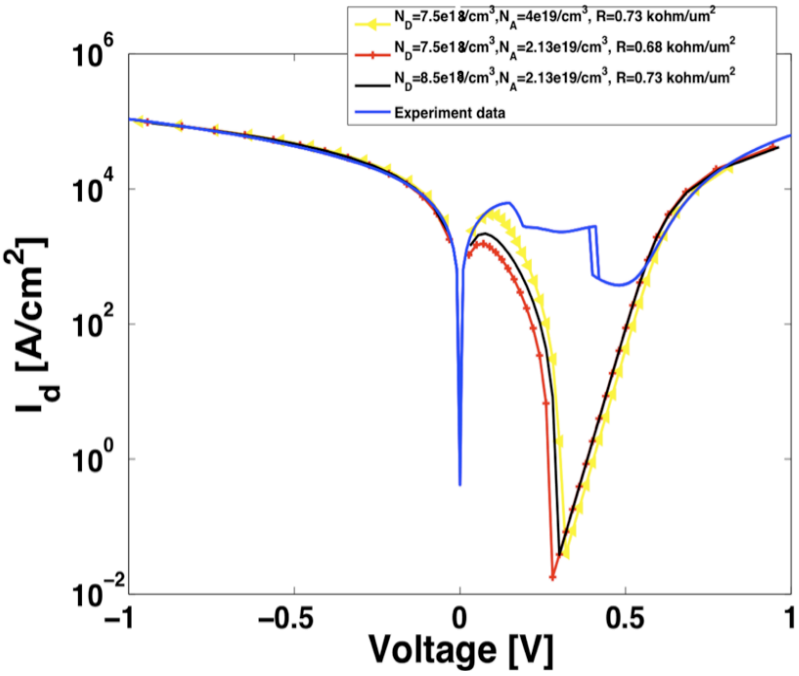

Fig. 4.24 The effect of higher donor (yellow line) and higher acceptor (black line) doping on the device current when BGN is included. The red line shows the simulated current using the doping profile extracted from SIMS measurement

The increase of the donor concentration has more effect on the increase of the peak current. However, for both cases, the Zener tunneling current also increases that they have even larger series resistance values. It seems that the modeling and simulation approach used for the device in the Case 1 is not quite valid in this case.

5. CONCLUSION AND FUTURE WORKS

In this thesis, homo-junction InGaAs p-n tunneling diodes lattice matched to InP were investigated. Devices fabricated at Penn State University and at Notre Dame University were reproduced using a full-band and atomistic quantum transport approach based on the tight-binding model and the Non-equilibrium Green's Function (NEGF) formalism. Band gap narrowing (BGN) is included in the tight-binding model by altering its parameters using the Jain-Roulston model. BGN is found to be critical in the determination of the current peak and the second turn-on in the forward bias region.

It was found that the experimental Zener tunneling branch (reverse-biased side) of the considered diodes could be relatively well reproduced by the simulation approach, contrary to the forward biased side. There, three important discrepancies could be observed (i) the simulated peak current is too small, up to 2 orders of magnitude, as compared to the experimental data, (ii) the simulated valley current is also too small, (iii) the turn-on of the simulated thermionic current occurs at too large biases. While the underestimation of the valley current can be explained by the absence of electron-phonon scattering in the simulation model, convincing explanations for the two other points are needed.

In a BTBT diode, transport through the junction is governed by the potential profile at the junction, and high impurity concentrations of the device influence the junction profile. Therefore, BGN effect due to high doping is considered in the modeling of the device. In this thesis, the Jain-Roulston model for the real band gap narrowing is included in tight-binding approach: the exact band gap narrowing of the n- and p- sides of the diodes were calculated as a function of their doping concentrations. The Jain-Roulston model treats the shift of the conduction and valence band separately. BGN is then included in the quantum transport simulations by shifting the band edges of the n- and p-

sides. As results, an increase of the peak current, closer to the experimental data, and an earlier turn-on of the thermionic current could be observed. However, purely ballistic NEGF calculations are found to be incapable to model BTBT diodes, and a careful investigation of the available experimental data suggested that the excess current through the gap states could contribute to the BTBT diode current. As results of adding empirical excess current to the ballistic simulated data, the closer current beyond the valley to the experiment are obtained.

However, it seems like this approach is only valid for the device fabricated at Penn State University. There are still problems with the contact series resistance R_S that must be attached to the intrinsic simulation domain for the device fabricated at Notre Dame University. To match the experimental data on the Zener tunneling side, values of R_S larger than estimated must be taken into account. This will be further investigated in the future, and another fabricated BTBT diode will be investigated to check the validity of the modeling approach used in this thesis. For more rigorous modeling, the temperature-dependence of BGN needs to be taken in account. More understanding of other high doping effects can lead us to estimate the sources of discrepancies between the experiment and simulation results. Also, the simulation including electron-phonon scattering will be conducted to improve the remaining discrepancy between the experimental and simulation results in the NDR region, and to expect the complete behavior of BTBT diodes.

When all these considerations are satisfied, and if the method of implementing BGN effect in other binary compound semiconductors are considered, we can apply these approach to any other high doping device structures including hetero-structure BTBT diodes and BTBT FETs.

LIST OF REFERENCES

LIST OF REFERENCES

[1] http://en.wikipedia.org/wiki/Moore's_law

[2] http://www.intel.com/technology/mooreslaw/

[3] http://software.intel.com/en-us/articles/gigascale-integration-challenges-and-opportunities/

[4] R. R. Schmidt, and B. D. Notohardjono, “High-End Server Low-Temperature Cooling”, *IBM J. Res. & Dev*., vol.46, No. 6, p. 739, 2002.

[5] S. M. Sze, and Kwok K. NG, “Physics of Semiconductor Devices”, 3ed 2007, *Wiley-Interscience*, p. 418.

[6] S. M. Sze, and Kwok K. NG, “Physics of Semiconductor Devices”, 3ed 2007, *Wiley-Interscience*, p. 48.

[7] S. M. Sze, and Kwok K. NG, “Physics of Semiconductor Devices”, 3ed 2007, *Wiley-Interscience*, p. 429.

[8] S. M. Sze, and Kwok K. NG, “Physics of Semiconductor Devices”, 3ed 2007, *Wiley-Interscience*, p. 419.

[9] S. M. Sze, and Kwok K. NG, “Physics of Semiconductor Devices”, 3ed 2007, *Wiley-Interscience*, p. 420.

[10] J. V. Morgan, and E. O. Kane, "Observation of Direct Tunneling in Germanium," *Phys. Rev. Lett.,* vol. 3, p. 466, 1959.

[11] S. M. Sze, and Kwok K. NG, “Physics of Semiconductor Devices”, 3ed 2007, *Wiley-Interscience*, pp. 424-427.

[12] A. G. Chynoweth, W. L. Feldmann, and R. A. logan, "Excess Tunnel Current in Silicon Esaki Junctions," *Phys. Rev,* vol. 121, No. 3, p. 684, 1961.

[13] E. O. Kane, "Theory of Tunneling," *Journal of Applied Physics,* vol. 32, No. 1, p. 83, 1961.

[14] Tatsuo Yajima, and Leo Esaki, "Excess Noise in Narrow Germanium p-n Junctions," *Journal of the physical society of Japan,* vol. 13, No. 11, p. 1281, 1958.

[15] E. F. Schubert, “Doping in III-V Semiconductors”, 1ed 1993, *Cambridge*, p. 45.

[16] D. K. Roy, "On the Prediction of Tunnel Diode I-V Characteristics," *Solid-State Electron.,* vol. 14, p. 520, 1971.

[17] S. M. Sze, and Kwok K. NG, “Physics of Semiconductor Devices”, 3ed 2007, *Wiley-Interscience*, p. 430.

[18] S. M. Sze, and Kwok K. NG, “Physics of Semiconductor Devices”, 3ed 2007, *Wiley-Interscience*, p. 431.

[19] Dietrich Meyerhofer, George A. Brown, and H. S. Sommers, Jr., "Degenerate Germanium. I. Tunnel, Excess, and Thermal Current in Tunnel Diodes," *Phys. Rev,* vol. 126, p. 4, 1962.

[20] E. F. Schubert, “Doping in III-V Semiconductors”, 1ed 1993, *Cambridge*, p. 42.

[21] J. W. Slotboom, H. C. De Graaff, "Measurements of bandgap narrowing in Si bipolar transistors," *Solid-State Electronics,* vol. 19, p. 857, 1976.

[22] E. F. Schubert, “Doping in III-V Semiconductors”, 1ed 1993, *Cambridge*, p. 49.

[23] G. D. Mahan, "Energy gap in Si and Ge: Impurity dependence," *J. Appl. Phys,* vol. 51, No. 5, p.2634, 1980.

[24] K. F. Berggren, and B. E. Sernelius, "Band-gap narrowing in heavily doped many-valley semiconductors," *Physical Review B,* vol. 24, No. 4, p. 1971, 1981.

[25] R. A. Abram, G. J. Rees, and B. L. H. Wilson, "Heavily doped semiconductors and devices," *Advances in Physics,* vol. 27, No. 6, p. 799, 1978.

[26] P. A. Sterne, and J. C. Inkson, “Comment on Energy gap in Si and Ge: Impurity dependence,”*J. Appl. Phys,* vol. 52, No. 10, p. 6432, 1981.

[27] J. del Alamo, S. Swirhun, and R. M. Swanson, “Simultaneous measurement of hole lifetime, hole mobility and bandgap narrowing in heavily doped n-type silicon,” *IEDM Tech. Dig*., p. 290, 1985.

[28] S. C. Jain, and D. J. Roulston, "A simple expression for band gap narrowing (BGN) in heavily doped Si, Ge, GaAs, and GexSi1-x strained layers," *Solid-State Electronics,* vol. 34, No. 5, p. 453, 1990.

[29] S. C. Jain, and D. J. Roulston, "Band-gap narrowing in novel III-V semiconductors," *J. Appl. Phys,* vol. 68, No. 7, p.3747, 1990.

[30] Juan M. Lopez-Gonzalez, "The importance of bandgap narrowing distribution between the conduction and valence bands in abrupt HBT's," *IEEE Transactions on electron devices,* vol. 44, No. 7, p.1046, 1997.

[31] M. Lusier, A. Schenk, W. Fichtner, and G. Klimeck, "Atomistic simulation of nanowires in the sp3d5s* tight-binding formalism: From boundary condition to strain calculations," *Phys. Rev. B,* vol. 74, No. 20, p. 205323, 2006.

[32] S. C. Jain, J. M. McGregor, and D. J. Roulston, and P.Balk, "Modified Simple Expression for Bandgap narrowing in n-type GaAs," *Solid-State Electronics,* vol. 35, No. 5, p. 639, 1992.

[33] James C. Li, Marko Sokolich, Tahir Hussain, and Peter M. Asbeck, "Physical modeing of degenerately doped compound semiconductors for high-performance HBT design," *Solid-State Electronics,* vol. 50, pp. 1440-1449, 2006.

[34] S. Adachi, “Material Parameters of $In_{1-x}Ga_xAs_yP_{1-y}$ and related binaries”, *J. Appl. Phys,* vol. 53, p.8775, 1982.

APPENDIX

A. BAND SHIFTS BY JAIN-ROULSTON BGN MODEL

CALCULATIONS[28-30]:

In their theory, the equations are derived by identifying the 4 contributions to BGN: shift of the majority band edge due to exchange energy ($\Delta E_{ex(maj)}$), correlation energy shift of the minority band edge ($\Delta E_{cor(mino)}$), and carrier-impurity interaction shifts of the two band edges ($\Delta E_{int(maj)}$, $\Delta E_{int(mino)}$).

$$\Delta E_g = \Delta E_{ex(maj)} + \Delta E_{cor(mino)} + \Delta E_{int(maj)} + \Delta E_{int(mino)} \tag{A.1}$$

where

$$\frac{\Delta E_{ex(maj)}}{R} = 1.83\frac{\Lambda}{N_b^{1/3}}\frac{1}{r_s} \tag{A.1}$$

$$\frac{\Delta E_{cor(mino)}}{R} = \frac{0.95}{r_s^{3/4}} \tag{A.2}$$

$$\frac{\Delta E_{i(maj)}}{R} = \frac{1.57}{N_b r_s^{3/4}} \tag{A.3}$$

$$\frac{\Delta E_{i(mino)}}{R} = \frac{R_{(mino)}}{R}\frac{1.57}{N_b r_s^{3/4}} \tag{A.4}$$

Therefore, the total band gap narrowing is expressed as

$$\frac{\Delta E_g}{R} = 1.83\frac{\Lambda}{N_b^{1/3}}\frac{1}{r_s} + \frac{0.95}{r_s^{3/4}} + [1 + \frac{R_{(mino)}}{R}]\frac{1.57}{N_b r_s^{3/2}} \tag{A.5}$$

Multiplying effective Rydberg energy R, the above equations can be rewritten in the following forms.

$$\Delta E_{\text{ex(maj)}} \simeq \frac{0.21\times10^{-6}\Lambda}{\varepsilon_r N_b^{1/3}} N^{1/3} = \frac{0.21\Lambda}{\varepsilon_r N_b^{1/3}}\left(\frac{N}{10^{18}}\right)^{1/3} \tag{A.6}$$

$$\Delta E_{\text{cor(mino)}} \simeq \frac{1.1473\times10^{-5} m_d^{0.25}}{\varepsilon_r^{1.25}} N^{1/4} = \frac{0.3628 m_d^{0.25}}{\varepsilon_r^{1.25}}\left(\frac{N}{10^{18}}\right)^{1/4} \tag{A.7}$$

$$\Delta E_{\text{i(maj)}} \simeq \frac{1.6829\times10^{-11}}{N_b \varepsilon_r^{0.5} m_d^{0.5}} N^{1/2} = \frac{0.0168}{N_b(\varepsilon_r m_d)^{0.5}}\left(\frac{N}{10^{18}}\right)^{1/2} \tag{A.8}$$

$$\Delta E_{\text{i(mino)}} \simeq \frac{1.6829\times10^{-11} m_{d(\text{mino})}}{N_b \varepsilon_r^{0.5} m_d^{1.5}} N^{1/2} = \frac{0.0168 m_{d(\text{mino})}}{N_b \varepsilon_r^{0.5} m_d^{1.5}}\left(\frac{N}{10^{18}}\right)^{1/2} \tag{A.9}$$

$$\Delta E_{\text{g}} = \frac{0.21\Lambda}{\varepsilon_r N_b^{1/3}}\left(\frac{N}{10^{18}}\right)^{1/3} + \frac{0.3628 m_d^{0.25}}{\varepsilon_r^{1.25}}\left(\frac{N}{10^{18}}\right)^{1/4} + \frac{0.0168}{N_b(\varepsilon_r m_d)^{0.5}}\left(1+\frac{m_{d(\text{mino})}}{m_d}\right)\left(\frac{N}{10^{18}}\right)^{1/2} \tag{A.10}$$

where

$$m_d = \frac{m^*}{m_0} \tag{A.11}$$

The BGN parameters of the equation 3.8 can be calculated from the equation A.10.

$$A = \frac{0.21\Lambda}{\varepsilon_r N_b^{1/3}} \times 10^{-6} \tag{A.12}$$

$$B = \frac{0.3628 m_d^{0.25}}{\varepsilon_r^{1.25}} \times 10^{-4.5} \tag{A.13}$$

$$C = \frac{0.0618}{N_b(\varepsilon_r m_d)^{0.5}}\left(1+\frac{m_{d(\text{mino})}}{m_d}\right) \times 10^{-9} \tag{A.14}$$

The total BGN can be separated into the majority and minority band shifts, and the constants in the equation 3.9 and 3.10 can be calculated from the following equations.

$$\Delta E_{\text{maj}} = \frac{0.21\Lambda}{\varepsilon_r N_b^{1/3}}\left(\frac{N}{10^{18}}\right)^{1/3} + \frac{0.0168}{N_b(\varepsilon_r m_d)^{0.5}}\left(\frac{N}{10^{18}}\right)^{1/2} \tag{A.15}$$

$$\Delta E_{\text{mino}} = \frac{0.3628 m_d^{0.25}}{\varepsilon_r^{1.25}}\left(\frac{N}{10^{18}}\right)^{1/4} + \frac{0.0168 m_{d(\text{mino})}}{N_b \varepsilon_r^{0.5} m_d^{1.5}}\left(\frac{N}{10^{18}}\right)^{1/2} \tag{A.16}$$

PARAMETERS:

Table A.1 $In_{0.53}Ga_{0.47}As$ parameters for BGN calculation[34]

	ε_r	m_d	$m_{d(mino)}$	m_{de}	m_{dh}	m_{hh}	m_{lh}	Λ	N_b
p-type	13.5	m_{dh}	m_{de}	0.041	0.61	0.6	0.05	0.75	2
n-type	13.5	m_{de}	$(m_{hh}+m_{lh})/2$	0.041	0.61	0.6	0.05	1	1

Table A.2 BGN parameters of p-$In_{0.53}Ga_{0.47}As$ to calculate the total BGN (calculated from the material parameters in Table A.1)

A	B	C
9.20×10^{-9}	3.57×10^{-7}	3.65×10^{-12}

Table A.3 Numerical BGN parameters of n-$In_{0.53}Ga_{0.47}As$ to calculate the total BGN

A	B	C
4.76×10^{-8}	9.99×10^{-8}	0

Table A.4 BGN parameters of $In_{0.53}Ga_{0.47}As$ to calculate each band shift

	C_1	C_2	C_3	C_4
n-type	0.0476	0	0.0032	0
p-type	0.0092	0.0034	0.0113	2.2988e-4